Biointerface Research in Applied Chemistry
Open-Access Journal (ISSN: 2069-5837)

Article
Volume 13, Issue 6, 2023, 527
https://doi.org/10.33263/BRIAC136.527

Synthesis Optimization and Sinterability of Nano Mg-Al-Layered Double Hydroxides Doped with Co or Ni Ions

Mahmoud F. Zawrah [1,*], Eman E. Ghanaym [1], Heba E.H. Sadek [1], Souria A. El Defrawy [1], Omyma A.M. Ali [2]

[1] National Research Centre, Refractories, Ceramics and Building Materials Department, 12622 Dokki, Cairo, Egypt; mzawrah@hotmail.com (M.F.Z.); eman_ghanaym@yahoo.com (E.E.G.); hsadek2004@yahoo.com (H.E.H.S); sa.elderawaye@gmail.com (S.A.E.)
[2] Faculty of women for Arts, Science and Education, Chemistry Department, Ain Shams University, Egypt; omyamaahmed92@yahoo.com (O.A.M.A.);
* Correspondence: mzawrah@hotmail.com; (M.F.Z.);

Scopus Author ID 6604055746
Received: 13.09.2022; Accepted: 4.11.2022; Published: 4.02.2023

Abstract: Recently, the synthesis and application of layered double hydroxides (LDHs) have received great interest. In this study, non-doped and Co-/Ni-doped nano Mg-Al-LDHs were prepared by co-precipitation coupled with the hydrothermal method. The synthesis parameters, such as type of alkaline medium, temperature, and concentration of dopants, were investigated and optimized. All prepared LDH nanopowders were inspected by the appropriate techniques as XRD, FT-IR, SEM, and TEM. The sinterability of prepared nano LDHs was studied to produce sintered spinel at a lower temperature than those prepared from micro-sized precursors published in the literature, which need a higher sintering temperature. The prepared nano LDHs powders were calcined, pressed, and sintered at 1500 ^{o}C. The sintered bodies were also examined by suitable tools such as XRD, SEM, and physical properties measurements. The results revealed that non-doped and doped nano LDHs were successfully prepared using NaOH solution rather than NH_4OH solution. Nano LDHs is an excellent precursor for producing sintered spinel at a lower temperature (1500 ^{o}C) with significant properties. The microstructures of sintered spinel exhibited nano grains agglomerated together. The spinel doped with nickel showed the highest sintering parameters.

Keywords: nano LDH; hydrothermal synthesis; spinel; sintering; properties.

1. Introduction

LDHs, or hydrotalcite-like compounds (HTCs), have received great interest owing to their layered structure and high anion exchange capability [1]. They are considered hydroxyl carbonates of Mg and Al under the anionic-clay category with the chemical formula of $Mg_6Al_2(OH)_{16}CO_3{\cdot}4H_2O$ [2]. Their conversion into sintered ceramic gives an important category named spinel-containing composites, which have many applications starting from engineering structural and refractory materials to electronics and medical applications [4-6]. The structure of LDH is analogous to brucite $Mg(OH)_2$ with a divalent metal-cation in the midpoint of octahedral $M(OH)_6$. Every two-edged $M(OH)_6$ octahedron forms two dimension layered sheet structures. Fractional replacement of trivalent cations for divalent ones tends to have a positive charge on the layers which are neutralized by the organic- or inorganic anions. The water of crystallization is also normally created between the interlayers [7, 8]. The known

formula of LDHs is $[L^{(II)}_{1-x}L^{(III)}_{x}(OH)_2]^{+}[A^{n-}]x/n.yH_2O$ [2]; since LII denotes a divalent-metal like Mg^{2+}, Ni^{2+}, Co^{2+}, Fe^{2+}, Cu^{2+}, Zn^{2+}, Ca^{2+} etc.; LIII is a trivalent-metal like Al^{3+}, Co^{3+}, Fe^{3+}, Mn^{3+}, Ga3+, Cr^{3+}, La^{3+} etc. and An^{-} is an anion as Cl^{-}, F^{-}, CO_3^{2-}, NO^{3-} etc.; and x lies between 0.25 and 0.33. So, the following formula is probable to be formed $[L^{(II)}_{0.75}L^{(III)}_{0.25}(OH)_2][A^{n-}]_{x/n}.yH_2O$ to $[L^{(II)}_{0.67}L^{(III)}_{0.33}(OH)_2][A^{n-}]_{x/n}.yH_2O$ or $[L^{(II)}_{2}L^{(III)}(OH)_6][A^{n-}]_{x/n}.yH_2O$ and $[L^{(II)}_{3}L^{(III)}(OH)_8][A^{n-}]_{x/n}.yH_2O$ which are considered as 2:1 LDHs or 3:1 LDHs, respectively. The values of y are ≤ 2. The amount of counter-anion (An-) depends on the charge of the anion, such that x/n achieves charge neutrality in the LDH structure [2]. During doping in octahedron sites, the radii should not exceed those of divalent and trivalent cations. LDH is a white-hydrated material having rhombohedral construction, small hardness (2.00), and small specific gravity (2.06) [9]. Many simple and low-cost synthetic approaches have been effectively utilized to prepare LDHs. The selection of preparation technique is preferred depending on the desired interlayer anions [10]. The recognized methods are co-precipitation or co-precipitation with hydrothermal treatment methods [11], ion exchange [10], reconstruction or rehydration using "Memory effect" [12-19], sol-gel, fast nucleation [20], urea precipitation, and microwave synthesis method. It is well known that the thermal decomposition of LDH structure at moderate temperature (300°C) increases its specific surface area [21, 22]. On the other hand, the sintering of material at high temperatures tends to cause a noticeable decrease in specific surface area.

Magnesium aluminate is the origin (normal) spinel, $MgAl_2O_4$ [23,24], in which divalent cation Mg^{2+} ion fills the tetrahedral sites and trivalent cation Al^{3+} ion occupies the octahedral positions in the cubic-closed packing of O^{2-} anions. The vacancies in the spinel structure assist the doping by transition metals and producing spinels with good characteristics. Owing to its serious properties, $MgAl_2O_4$ is doped with transition metals such as Co^{2+}, Ni^{2+}, Cu^{2+}, etc. has attracted huge attention from researchers and technologists [25]. Spinels having transition metals are colored and usually used as inorganic pigments. Magnesium aluminate ($MgAl_2O_4$), cobalt aluminate ($CoAl_2O_4$), and nickel aluminate ($NiAl_2O_4$) spinels have many interesting properties such as high melting point (2135°C, 1955°C, and ~2110°C), excellent electrical and mechanical properties; high hardness, high chemical stability, good optical characteristics, lower thermal expansion, adsorption behavior and good catalytic performance [26-36]. Although the synthesis, structural properties, and applications of $MgAl_2O_4$, $CoAl_2O_4$, and $NiAl_2O_4$ have been extensively investigated individually, little attention has been directed to studying the synthesis and characteristics of $MgAl_2O_4$–$NiAl_2O_4$ and $MgAl_2O_4$-$CoAl_2O_4$ solid solutions. Many researchers [38, 24] have examined the spreading of Ni-ion among octahedral and tetrahedral sites in $NiAl_2O_4$–$MgAl_2O_4$ solid solutions. When produced by solid-state reaction, most of these materials require high temperatures and long periods; for example, commercial $MgAl_2O_4$ is usually sintered at temperatures more than 1650°C for 2h to produce full sintered bodies when prepared by conventional solid-state methods [24, 25, 39].

It is challenging to prepare sintered spinels having no porosity from micro-sized materials using traditional methods at low temperatures owing to higher grain boundary energy which makes grain coarsening. Thus, the incorporation of sintering aids or utilizing nano-sized precursors, or elevating the sintering temperature are the main factors controlling the sintering process. The preparation of spinel through LDHs leads to obtaining rich divalent metal ions, which facilitate the sintering process. Moreover, excess divalent cations restrict grain growth and enhance the sintering process. Many researchers have studied the sintering of spinels prepared from different sources [40], but few studies have been conducted on the sintering of

spinel prepared from LDHs [41, 42]. In those studies, the researchers succeeded in preparing porous sintered Mg-Al spinel using LDHs. Therefore, the objectives of the present study are to optimize the synthesis conditions and sintering of nano Mg-Al-layered double hydroxides doped with Co or Ni ions to obtain densely sintered spinel. Both synthesized nanopowders and sintered bodies are subjected to full characterization by different tools.

2. Materials and Methods

2.1. Materials.

The entire chemicals; magnesium-nitrate $Mg(NO_3)_2 \cdot 6H_2O$, nickel-nitrate $Ni(NO_3)_2 \cdot 6H_2O$, cobalt nitrate $Co(NO_3)_2 \cdot 6H_2O$, aluminum nitrate $Al(NO_3)_3 \cdot 9H_2O$, sodium hydroxide NaOH, ammonium hydroxide NH_4OH and sodium carbonate Na_2CO_3 utilized in the current work were ultra-pure grade and supplied by Sigma Aldrich.

2.2. Synthesis of MgAl-CO_3-LDH using NaOH.

The original MgAl-CO_3-LDH was prepared by the co-precipitation method as described by Miyata [43,44], followed by hydrothermal treatment [45, 46]. Figure 1 shows the flowchart for the preparation of LDH. Typically, about 38.463 g of $Mg(NO_3)_2 \cdot 6H_2O$ and 18.762 g of $Al(NO_3)_3 \cdot 9H_2O$ were dissolved in 180 ml deionized water (denoted as Solution A) to give 2:1 (Mg^{2+}/Al^{3+}) molar ratio. In another container, 13.64 g NaOH and 11.31 g Na_2CO_3 were dissolved in 80 ml deionized water (symbolized as Solution B). At room temperature, solution-B was added to solution-A with energetic stirring, keeping the pH value of the mix at about 10. The resulting suspension (formed as a white precipitate gel) was centrifuged at a rate of 6000 rpm six times and washed with deionized water; then divided into three portions; the first part was dried at 70 °C for 24 h in an oven (sample a), while the second and third parts were washed and retained in a small amount of distilled water as is then put in a Teflon stainless autoclave and hydrothermally treated in an oven at 140 and 180 °C for 24 h (samples b and c), respectively, for LDH formation. Afterward, the autoclave was cooled to ambient temperature, and the formed LDHs were collected. This work was followed by synthesizing of Mg-Al-CO_3-LDH doped with different ratios (10, 20, and 30%) of Ni^{2+} or Co^{2+} by the same aforementioned methods using $Mg(NO_3)_2 \cdot 6H_2O$ & $Ni(NO_3)_2.6H_2O$ or $Co(NO_3)_2.6H_2O$ and $Al(NO_3)_3 \cdot 9H_2O$ with a molar ratio of (MII): Al^{3+} (MIII) equal 2:1 at pH value ca. 10, since (MII = Mg^{2+} (Ni^{2+} or Co^{2+})). The ratios of Ni^{2+}or Co^{2+}: Mg^{2+} in the prepared samples were (15.15 : 84.8), (33 : 66), and (45.5 : 54.5). In other words, the Al^{3+} ion ratio was still constant during the reaction while that for Mg^{2+} decreases by replacing Ni^{2+}or Co^{2+}. The ratios of (Mg^{2+}: Ni^{2+} or Co^{2+}: Al^{3+}) in all suggested compounds were (50.6 : 10 : 33.3), (40.6 : 20 : 33.3) and (30.6 : 30 : 33.3). The steps for preparation of LDHs doped with different ratios of (MII) were as the previously mentioned with only one difference that the solution A contained a mixture of $Mg(NO_3)_2 \cdot 6H_2O$ & $Ni(NO_3)_2.6H_2O$ or $Co(NO_3)_2.6H_2O$ and $Al(NO_3)_3 \cdot 9H_2O$ with the same molar ratios as mentioned before and autoclaved at 180 oC for 2 h. In order to examine the effect of heat treatment on the changes in phases and morphology, the synthesized LDH was calcined at 400, 600, 800, and 1000 °C for 2 h.

2.3. Synthesis of MgAl-CO_3-LDH using NH_4OH.

Solution A was prepared as previously mentioned in this method, and NH_4OH was used to reach the desired pH value. Typically, 11.31 g Na_2CO_3 was dissolved in 40 ml of deionized water. At room temperature, a three-necked flask containing solution-A, Na_2CO_3 solution, and NH_4OH solution, was added to solution-A with dynamic stirring, preserving the pH value of the mix at about 10. The produced white suspension was centrifuged at 6000 rpm and washed with deionized water several times. The washed precipitate was divided into three portions; the first part was dried at 70 °C for 24 h in an oven (sample a), while the second and third parts were added to a small amount of distilled water and put in Teflon stainless autoclave and treated hydrothermally in an oven at 140 and 180 °C for 24 h (sample a and b), respectively for LDH formation. Afterward, the autoclave was cooled at ambient temperature, and the synthesized LDH was collected. Table 1 illustrates the weights of starting materials used to prepare pure LDHs and those doped by Ni or Co with their expected formula.

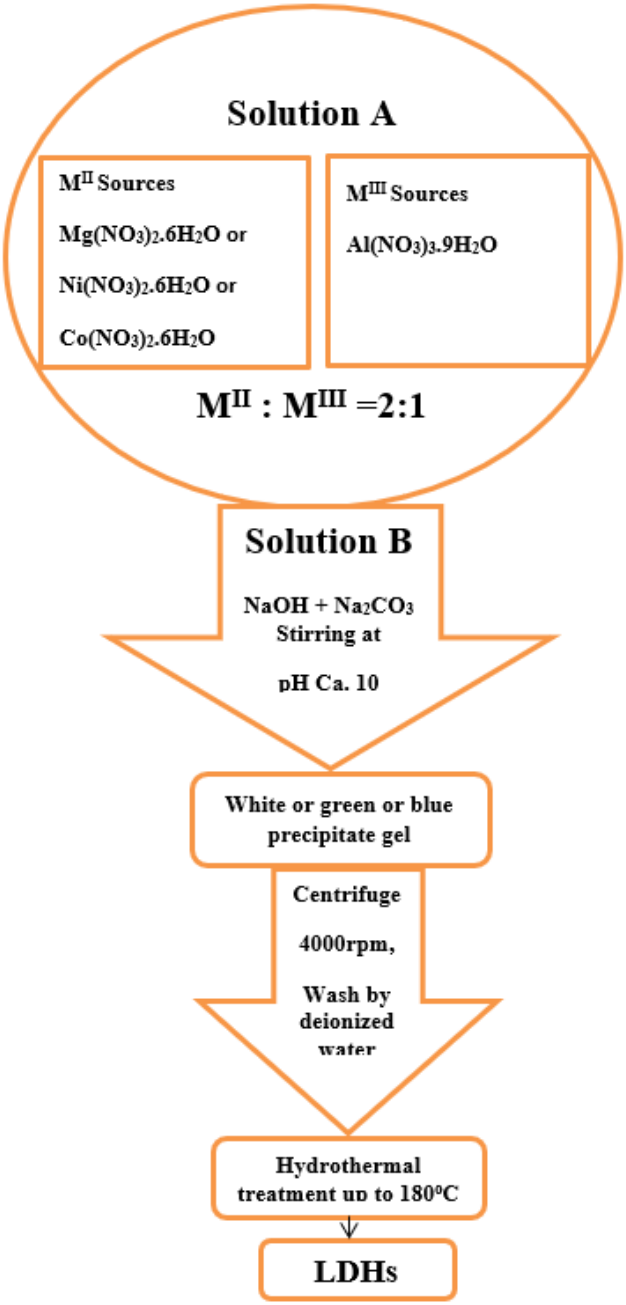

Figure 1. Flowchart for preparation of LDH.

Table 1. Weights of starting materials used for the preparation of LDHs from pure chemicals using NaOH and those doped by Ni or Co with their expected formula.

Sample identification	Expected LDH formula	$Mg(NO_3)_2 \cdot 6H_2O$		$Ni(NO_3)_2 \cdot 6H_2O$		$Co(NO_3)_2 \cdot 6H_2O$		$Al(NO_3)_3 \cdot 9H_2O$	
		Mg^{2+}, %	Wt., g	Ni^{2+}, %	Wt., g	Co^{2+}, %	Wt., g	Al^{3+}, %	Wt., g
As-synthesized LDH prepared using NaOH	$[Mg_{0.66}Al_{0.33}(OH)_{16}](CO_3)_{0.167}.4(H_2O)_{0.5}$	66.6	38.46					33.3	18.76
LDH doped with 10% Ni^{2+}	$[Mg_{0.567}Ni_{0.1}Al_{0.333}(OH)_{16}](CO_3)_{0.167}\cdot 4H_2O_{0.5}$	50.6	17.80	10	3.56			33.3	15.29
LDH doped with 20% Ni^{2+}	$[Mg_{0.467}Ni_{0.2}Al_{0.333}(OH)_{16}](CO_3)_{0.167}\cdot 4H_2O_{0.5}$	40.6	14.06	20	6.83			33.3	14.67
LDH doped with 30% Ni^{2+}	$[Mg_{0.367}Ni_{0.3}Al_{0.333}(OH)_{16}](CO_3)_{0.167}\cdot 4H_2O_{0.5}$	30.6	10.62	30	9.85			33.3	14.1
LDH doped with 10% Co2+	$[Mg_{0.567}Co0.1Al_{0.333}(OH)_{16}](CO_3)_{0.167}\cdot 4H_2O_{0.5}$	50.6	17.79			10	3.56	33.3	15.28
LDH doped with 20% Co2+	$[Mg_{0.467}Co_{0.2}Al_{0.333}(OH)_{16}](CO_3)_{0.167}\cdot 4H_2O_{0.5}$	40.6	14.06			20	6.83	33.3	14.66
LDH doped with 30% Co2+	$[Mg_{0.367}Co_{0.3}Al_{0.333}(OH)_{16}](CO_3)_{0.167}\cdot 4H_2O_{0.5}$	30.6	10.61			30	9.85	33.3	14.09

2.4. Characterization of prepared LDH powders.

Phase identification of as-prepared and calcined (400, 600, 800, and 1000 °C) pure and doped LDHs with Ni^{2+} or Co^{2+} was conducted using the x-ray diffraction tool model "Philips PW 1373" with CuKα-Ni target. The phase fractions of the obtained phases were determined by XRD semi-quantitative analysis. The crystal sizes of as-prepared LDHs were estimated using the Scherrer equation [47-49], according to the obtained XRD data using the following formula:

$$D = \frac{0.9\lambda}{BCos\theta} \quad \ldots\ldots\ldots\ldots\ldots\ldots\ldots\ldots\ldots\ldots (1)$$

where λ=1.5418 °A (wavelength) for Cu-Ni radiation, B is the full width at half maximum (FWHM) and θ is the angle in radians.

To confirm the structure and composition of synthesized LDH, FT-IR spectroscopy model Vertex 70 was utilized at ambient temperature in the wave number range 4000-400 cm^{-1}.

Scanning electron microscopy model SEM Inspect-S, T810-D8571, FEI Co., Japan, operated at 30kv acceleration volt with ultra-high magnification, was used to explore the shape and particle size of prepared LDHs. The samples were coated with a gold thin film before investigation. On the other hand, transmission electron microscopy model JEOL JEM-1230 was used to examine the shape and particle size of as-prepared LDHs suspension after ultra-sonication for 30 min before investigation.

2.5. Sintering of prepared LDHs.

The starting pure and doped LDHs powders calcined at 1000 °C were uni-axially compacted at 100 MPa to achieve samples of 2.54 cm diameter and 1.27 cm thickness. Then, the samples were sintered in a normal atmosphere at 1500 °C as the temperature was elevated at the rate of 8 degrees per minute from room temperature up to 1000 °C, then 5 °C/min up to the maximum temperature, then held for 2 h.

2.6. Characterization of sintered materials.

The changes in phase composition of sintered specimens were identified by XRD analysis (as previously mentioned) after grinding the sintered pellets to a fine powder in an agate mortar. The physical properties in terms of bulk density and apparent porosity of sintered pellets were examined by the Archimedes displacement method. The pellets under examination were soaked in distilled water under air vacuum suction for 1 h to get rid of the air found in the pellets and displaced with water. Microstructure features of sintered pellets were examined using a scanning electron microscope (Type: previously mentioned). The pellets were coated with thin gold film before investigation.

3. Results and Discussion

3.1. Properties of synthesized LDHs from pure chemicals.

For the production of Mg-Al-LDH by hydrothermal treatment, several parameters control its formation. These include the amount of substitution for divalent cations (e.g., Mg) with trivalent ones (e.g., Al), the type of interlayer-anion, the pH of the solution (it increases till the desired pH at which the LDH is precipitated) and, in some cases, the reaction atmosphere [42, 50]. The preparation of Mg-Al-LDH using the reaction between magnesium nitrate and aluminum nitrate aqueous solution at pH ~ 4-6) can be represented by the following reactions:

$6Mg(NO_3)_2 + 2Al(NO_3)_3 + nH_2O \rightarrow 6Mg^{2+}(aq.) + 2Al^{3+}(aq.) + 18(NO_3)^{-}(aq.) + mOH^{-}$

As the pH increases (by the addition of Na_2CO_3, NaOH, or NH_4OH), the reaction proceeds as follows:

$6Mg^{2+}(aq.) + 2Al^{3+}(aq.) + 18\,(NO_3)^{-}\,(aq.) + mNa^{+}(aq.)$ or $m(NH_4)^{-}(aq.) + m(CO_3)^{2-}(aq.) + mOH^{-} \rightarrow (Mg_6Al_2(OH)_{16}(CO_3)\cdot 4H_2O)$ (precipitated) + $NaNO_3$ or NH_4NO_3

The net result equation is:

$6Mg(NO_3)_2 + 2Al(NO_3) + NaOH$ or $NH_4OH + Na_2CO_3 \rightarrow (Mg_6Al_2(OH)_{16}(CO_3)\cdot 4H_2O) + NaNO_3$ or NH_4NO_3

3.1.1. Phase composition of LDHs synthesized using aqueous NaOH:

Figure 2 displays XRD patterns of as-synthesized LDH using aqueous NaOH at various temperatures; (a) as-synthesized and dried at 75 °C (b) synthesized at 140 °C, and (c) synthesized at 180 °C. It is noted that pure LDH is successfully prepared with dissimilar crystallinity at 75, 140, and 180 °C after a period of 24 h [48]. LDH prepared at 180 °C shows the highest crystallinity since it displays higher intensity and harsh peaks. The percentage of peaks' intensities of LDH synthesized at 75, and 140 °C as compared to that synthesized at 180°C are 87.12 and 12.87 %, respectively. This indicates that increasing the temperature leads to improving the crystallinity in this process [52]. As detected in the XRD chart, the typical peaks of crystalline-LDH seem to be at $2\theta = 11.52, 23.27, 34.71, 39.18, 45.8, 60.61$, and $61.91°$ (JCPDS file No: 00-014-0191). Mostly, crystallinity enhancement may be realized in water vapor at temperatures lower than the decomposition temperature of LDH, typically up to 200 °C for 1 - 24h under autogenous pressure [52]; this idea has been reported by Miyata [53]. The larger crystal size is achieved for the sample treated for 24h at 180 - 200 °C. Due to the growth that occurred at the edges, hexagonal-plate sheets are formed. Several researchers [53-58] reported on the parameters affecting the crystallinity of LDH and $MgAl_2O_4$ spinel hydrothermally prepared. They indicated that long reaction time and temperature at about 200

°C with the presence of pressure led to crystallinity development due to water being higher than the mother liquid. The crystal size of LDH prepared at 180 °C is found to be 28.52 nm.

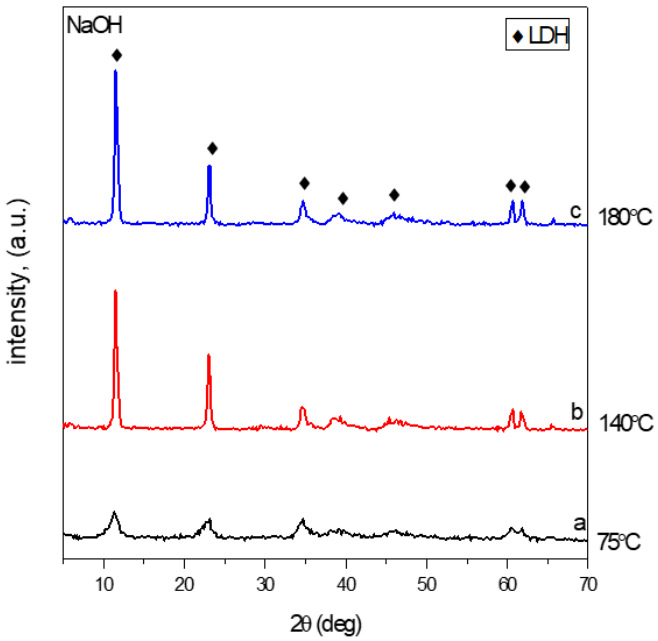

Figure 2. XRD patterns of LDHs prepared using aqueous NaOH at different temperatures **(a)** dried in the oven at 75°C for 24 h, **(b)** hydrothermally treated at 140, and **(c)** hydrothermally treated at 180°C for 24 h.

3.2. Phase composition of LDHs synthesized using aqueous NH_4OH.

In this section, for comparison and selection of the best method to synthesize LDHs, LDH was synthesized using aqueous NH_4OH instead of NaOH at the same conditions. Figure 3 depicts typical XRD patterns of as-synthesized LDH at various temperatures using an aqueous NH_4OH: (a) as-synthesized and dried at 75°C (b) hydrothermally treated at 140 °C and (c) hydrothermally treated at 180 °C. It is indicated that the characteristic peaks of the Mg-Al-CO_3-layered double hydroxide phase are not detected in the as-synthesized LDH and dried at 75°C. An unnamed mineral with the general formula $[NR]Al_5(OH)13CO_3.xH_2O$ appeared in this sample [51].

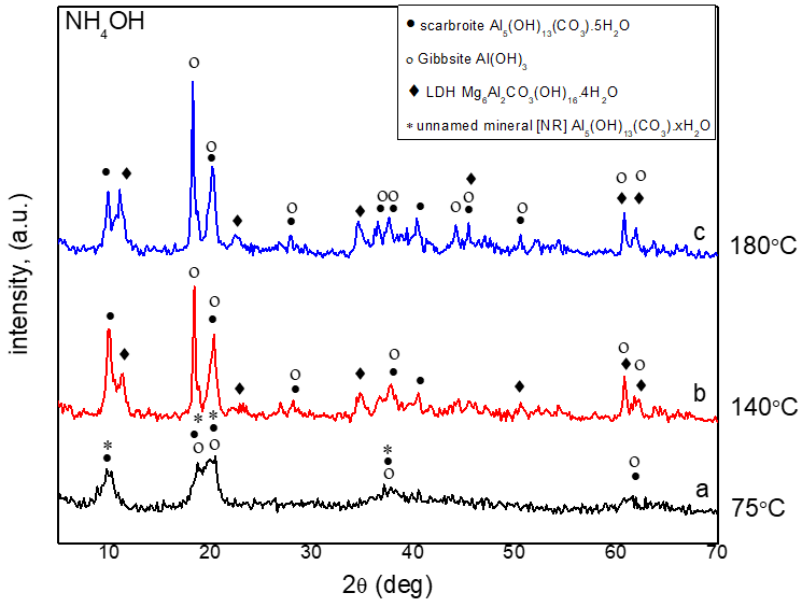

Figure 3. XRD patterns of LDHs prepared using aqueous NH_4OH at different temperatures **(a)** dried in the oven at 75°C for 24 h, **(b)** hydrothermally treated at 140, and **(c)** hydrothermally treated at 180°C for 24 h.

On the other hand, LDHs synthesized by hydrothermal treatment at 140 and 180°C for 24 h reaction time exhibit no pure LDHs but combined with other compounds formed during the reaction, such as scarbroite $Al_5(OH)_{13}CO_3.5H_2O$ at 2θ equal 9.88, 20.21, 27.7, 36.44, 37.6, 40.19, 45.57, 50.59, 60.73 and 62.03°, Gibbsite $Al(OH)_3$ at 2θ equal 18.2, 20.21, 27.7, 36.44, 37.6, 44.18, 45.57, 50.59, 60.73 and 62.03° and unnamed mineral $[NR]Al_5(OH)_{13}CO_3.xH_2O$ at 2θ equal 9.88, 18.2, 20.21, and 37.6°. As indicated from XRD patterns, the synthesized LDH has low crystallinity since lower peak intensities are detected at 2θ equal to 11.09, 22.41, 34.48, 45.57, 60.73, and 62.03°. This means that the synthesis of LDHs using aqueous NH_4OH is not preferable, while that prepared by aqueous NaOH is ideal, so it was selected for all preparations in the present work.

3.3. Phase composition of LDHs doped with different Ni^{2+} ratios.

Figure 4 depicts XRD patterns of synthesized LDHs doped with different Ni^{2+} ratios (a; 10, b; 20, and c; 30 %) from pure chemicals after autoclaving at 180 °C for 24 h. The close radii of Ni^{2+} (0.069 nm) and Mg^{2+} (0.072 nm) [62,63] facilitate the replacement of Mg^{2+} by Ni^{2+}. The figure shows that the diffraction peaks become broader and less intense with increasing nickel content. This means that the crystallinity decreases with increasing nickel content. The characteristic peaks for the prepared LDH appeared as combined peaks of magnesium aluminum hydroxide carbonate hydrate $Mg_4Al_2(OH)_{12}(CO_3)_{0.5}(H_2O)_3$ and nickel aluminum carbonate hydroxide hydrate $Ni_2Al(OH)_6(CO_3)_{0.5}(H_2O)$. This leads to some shifting to lower 2θ values with increasing Ni2+ content. The characteristic peaks of Mg-Ni-Al-LDH appear at 2θ equal 11.91, 23.81, 34.78, 39.69, and 47.58°. The crystal sizes of as-prepared LDHs doped with Ni are represented in Table 2. It is indicated that it decreases with increasing Ni amount. Its values ranged between 26-25 nm.

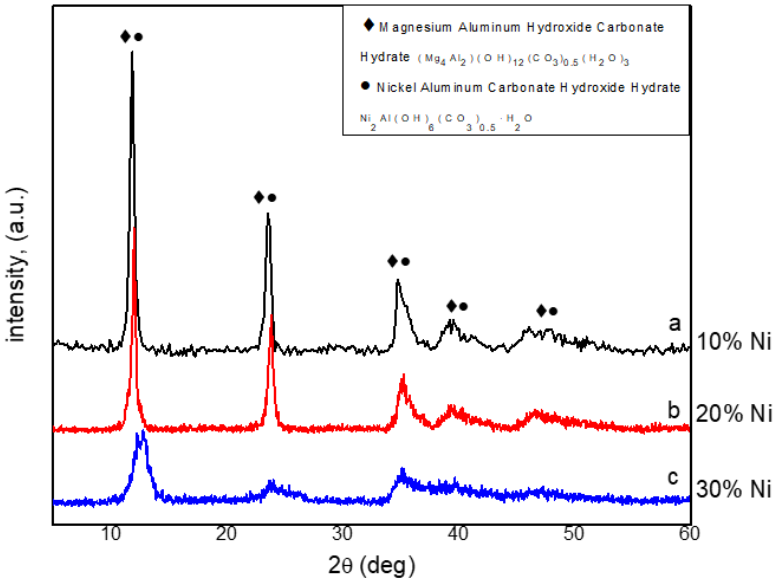

Figure 4. XRD patterns of LDHs doped with different Ni^{2+}ratios autoclaved for 24 h at 180°C.

Table 2. Crystallite size of synthesized LDHs doped with Ni^{2+}.

No.	Material type	Ni^{2+} content, %	Average crystal size, nm
1	$[Mg_{0.567}Ni_{0.1}Al_{0.333}(OH)_{16}](CO_3)_{0.167}\cdot 4H_2O_{0.5}$	10	27.66
2	$[Mg_{0.467}Ni_{0.2}Al_{0.333}(OH)_{16}](CO_3)_{0.167}\cdot 4H_2O_{0.5}$	20	26
3	$[Mg_{0.367}Ni_{0.3}Al_{0.333}(OH)_{16}](CO_3)_{0.167}\cdot 4H_2O_{0.5}$	30	25.04

3.4. Phase composition of LDHs doped with different Co^{2+} ratios.

By the same concept as previously mentioned, the near radii values of Co^{2+} (0.075 nm) and Mg^{2+} (0.072 nm) enable the replacement of Mg^{2+} by Co^{2+} [45,56,57]. Figure 5 shows XRD patterns of synthesized LDH doped with different Co^{2+} ratios (a; 10, b; 20, and c; 30%) after autoclaving at 180ºC for 24h. It also appeared that the diffraction peaks become broader and have weak intensity with increasing cobalt content; consequently, a decrease in crystallinity is obtained. The characteristic peaks for prepared LDHs are detected as a combined peak of magnesium aluminum hydroxide carbonate hydrate $Mg_4Al_2(OH)_{12}(CO_3)_{0.5}(H_2O)_3$ and cobalt aluminum carbonate hydroxide hydrate $Co_2Al(OH)_6(CO_3)_{0.5}(H_2O)$ with shifting to lower 2θ values as the cobalt content decreased. Generally, the shifting is appeared due to the change in crystal size. The characteristic peaks of Mg-Co-Al-LDH appear at 2θ equal 12.01, 23.81, 34.95, 39.59, and 46.56°. The crystallite sizes of synthesized LDHs doped with cobalt are illustrated in Table 3. It is indicated that the size decreases with increasing cobalt amount. Its values ranged between 20-26 nm.

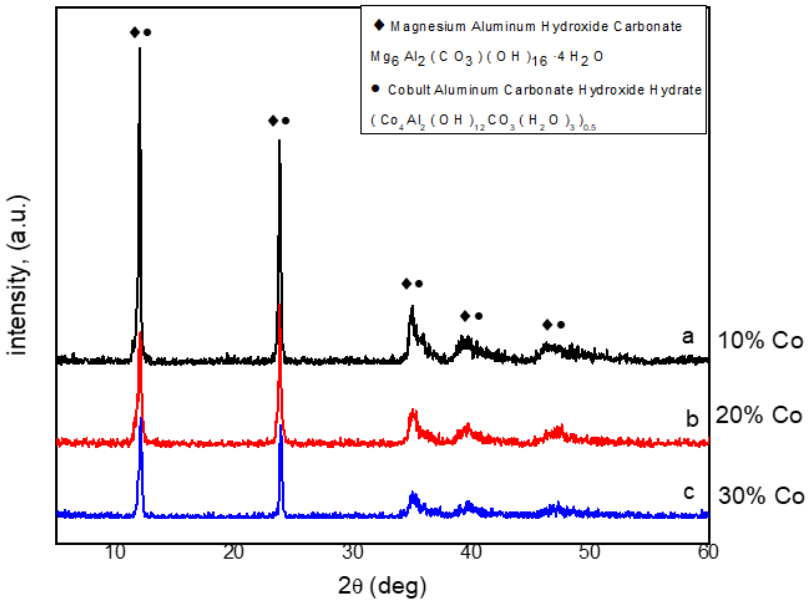

Figure 5. XRD patterns of LDHs doped with different Co^{2+} ratios autoclaved for 24 h at 180ºC.

Table 3. Crystallite size of synthesized LDHs doped with Co^{2+}.

No.	Material type	Co^{2+} content,%	Average crystal size, nm
1	$[Mg_{0.567}Co_{0.1}Al_{0.333}(OH)_{16}](CO_3)_{0.167}\cdot 4H_2O_{0.5}$	10	26.6
2	$[Mg_{0.467}Co_{0.2}Al_{0.333}(OH)_{16}](CO_3)_{0.167}\cdot 4H_2O_{0.5}$	20	25.8
3	$[Mg_{0.367}Co_{0.3}Al_{0.333}(OH)_{16}](CO_3)_{0.167}\cdot 4H_2O_{0.5}$	30	20.82

3.5. Phase composition of calcined LDHs.

It is important to investigate the phase changes of LDHs calcined at different temperatures by XRD. Figure 6 displays XRD patterns of LHD calcined at 400, 600, 800, and 1000 °C for 2h. For the sample calcined at 400 °C, it reserved layered structure while the inter-layer adsorbed water vanished at this temperature [61] with the occurrence of slight broad peaks conforming to MgO (periclase phase). The typical peaks of LDH are detected at 2θ = 11.42, 22.86, 34.58, 38.69, 45.73, and 52.05° but the peaks of MgO appeared at 2θ = 37.37 and 43.09°. Furthermore, the reflections of LDH are low compared to as-synthesized at 180°C, demonstrating the failure of a layered structure with the formation of a new phase. With rising temperatures up to 600 and 800 °C, the typical peaks of crystalline LDH convert into weak

peaks with the increasing intensity of MgO peaks. For the sample calcined at 1000°C, the LDH-phase vanishes, and some typical peaks of $MgAl_2O_4$ spinel appeared at 2θ = 19.17, 31.43, 37.05, and 44.99° [62]. At that temperature, migration of A1 ions from the Mg-A1 double hydroxide phase into a spinel phase ($MgA1_2O_4$) occurs, and then the double hydroxide decomposes.

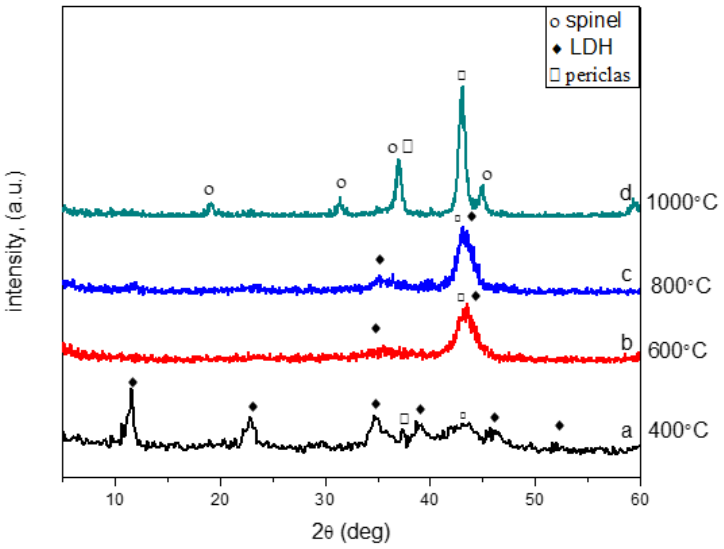

Figure 6. XRD patterns of pure LDHs calcined at different temperatures.

3.6. Phase composition of calcined LDHs doped with 30 % Ni^{2+}.

Figure 7 shows XRD patterns of LDHs doped with 30 % Ni^{2+} calcined at 400, 600, 800, and 1000 °C for 2h. For the sample thermally treated at 400°C, it keeps hold of layered-structure while the inter-layer adsorbed H_2O vanished in this step [61] with the existence of slight broad peaks consistent with bunsenite (NiO) and periclase (MgO) phases. The typical reflections of LDH seem at 2θ=11.72, 23.57, and 35.6° whereas the peaks of MgO and NiO are noticed at 2θ = 43.37°.

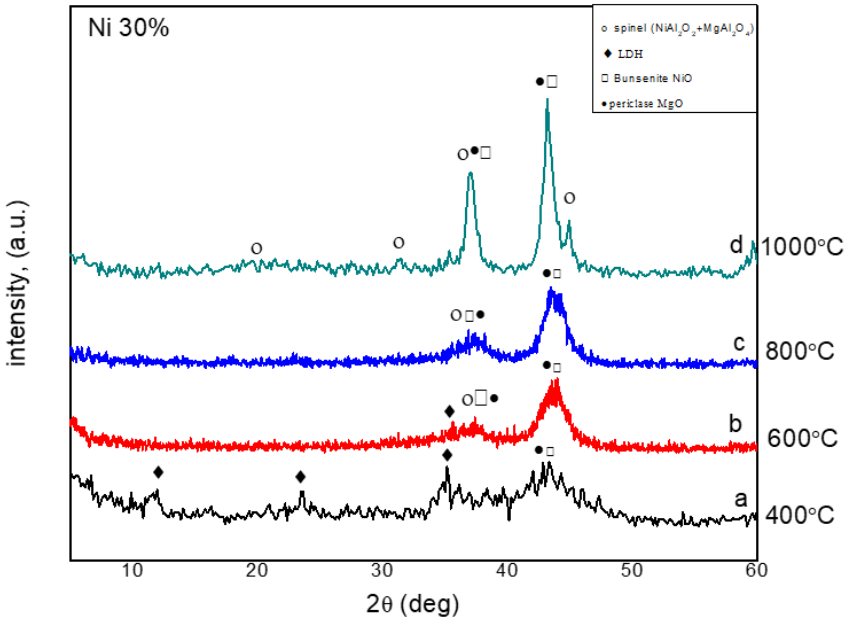

Figure 7. XRD patterns of LDHs doped with 30% Ni^{2+} calcined at different temperatures.

Also, for the sample calcined at 400 °C, the reflections of LDH turned into small reflections compared with that of as-synthesized at 180 °C, demonstrating the collapse of the layered structure with the formation of the new phase. The characteristic reflections of crystalline LDH became much weaker at 600 and disappeared at 800 °C. After increasing the temperature to 600 and 800 °C, the intensity of periclase and bunsenite peaks increased, and some typical peaks of $MgAl_2O_4$ and $NiAl_2O_4$ spinels appeared at 2θ=37.35° [62]. At 1000°C, there is an increase in the intensity of the characteristic peaks for bunsenite NiO and periclase MgO at 2θ equal 37.04 and 43.23°.This is due to the decomposition of formed double hydroxide into spinel, MgO, or NiO. Also, the peaks of $MgAl_2O_4$ and $NiAl_2O_4$ spinels appear at 2θ equal 19.7, 31.12, 37.04, 44.86, and 59.44°. This indicates that the replacement between Ni^{2+} and Mg^{2+} leads to a $NiMgAl_2O_4$ solid solution [63].

3.7. Phase composition of calcined LDHs doped with 30 % Co^{2+}.

Fig. 8 shows XRD patterns of LDH doped with 30 % Co^{2+} calcined at 400, 600, 800, and 1000 °C for 2h. In the case of cobalt addition, a relatively similar behavior to that of nickel is obtained after calcination at 400 °C with a small broad reflection corresponding to cobalt oxide CoO and a big reflection peak corresponding to MgO. The typical reflections of LDH are looked at 2θ = 11.34, 22.34, 34.5, and 38.8° whereas the peaks of MgO and CoO are noticed at 2θ = 36.90 and 42.97°. Also, for the sample calcined at 400 °C, the reflections of LDH turned into small peaks compared with that of as-synthesized at 180 °C, signifying the collapse of a layered structure with the formation of new phases. The characteristic reflections of crystalline LDH disappeared at 600°C. With increasing the temperature to 600, 800, and 1000 °C, the intensity of periclase and cobalt oxide peaks increases and appears at 2θ=37.1 and 43.02°. Some characteristic reflections of $MgAl_2O_4$ and $CoAl_2O_4$ spinels are detected at the same reflections at 2θ =19.2, 31.5, 37.1, 44.99, and 55.9° [62]; their intensities increase with increasing temperature. This means that $MgCoAl_2O_4$ spinel solid solution is formed [63].

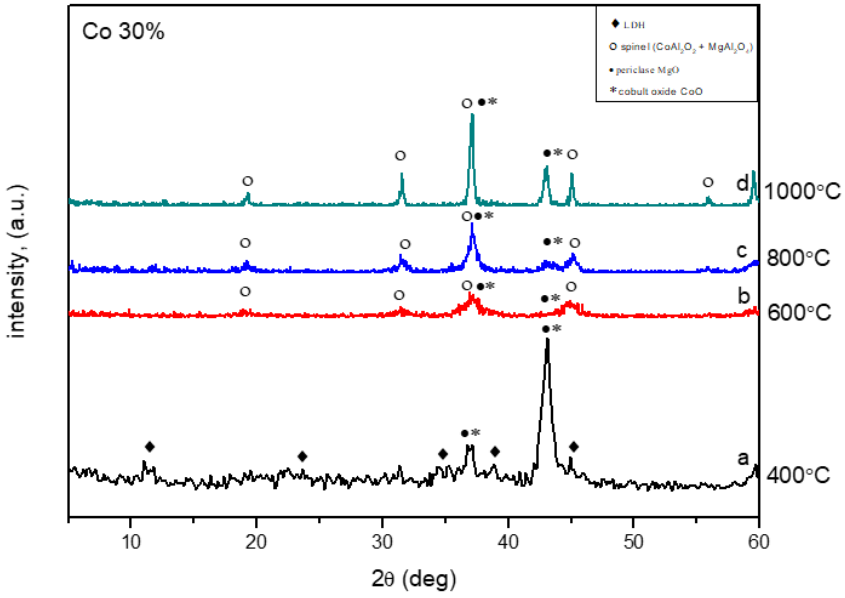

Figure 8. XRD patterns of LDHs doped with 30% Co^{2+} calcined at different temperatures.

For comparison, Fig. 9 exhibits XRD patterns of LDHs calcined at 1000 ºC doped with 30% Ni^{2+} or Co^{2+}. It is indicated that the peak intensity increases in the following order, LDH doped 30% Co < LDH doped with Ni < Pure LDH. This means that the crystal size of LDH

doped 30% Co < LDH doped with Ni < Pure LDH; which is reflected consequently in the sinterability of these materials as discussed later.

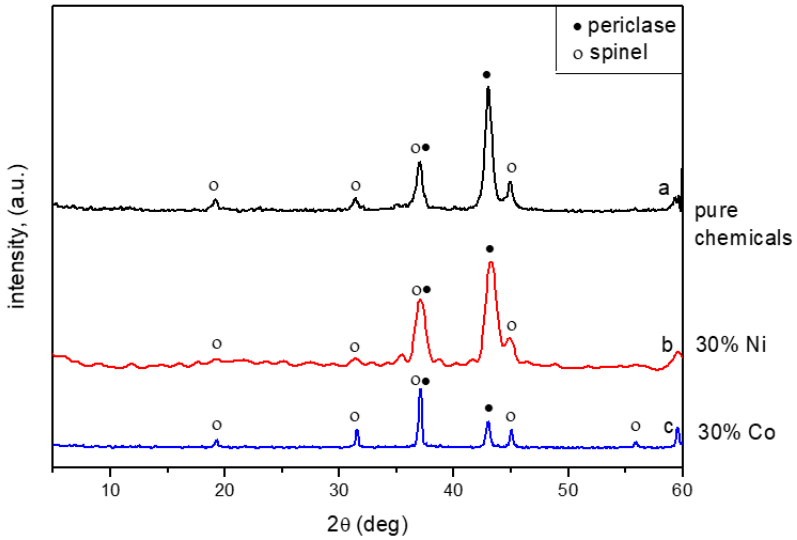

Figure 9. XRD patterns of LDHs calcined at 1000ºC (**a)** pure LDH, (**b)** doped with 30% Ni^{2+}, and (**c)** doped with 30% Co^{2+}.

3.8. FT-IR for pure LDHs.

Figure 10 displays FT-IR spectra of as-prepared pure LDH that calcined at various temperatures. Comparable spectra with some nonconformity appeared for all samples. The bands at 3470 and 1646 cm^{-1} are allocated to the characteristic OH stretching and bending vibrations of the layered structure's inter-layer H_2O molecule and OH groups [64,65]. After raising the temperature from 180 to 1000 °C, the band intensity is reduced owing to the evaporation of inter-layer H_2O molecule or dehydroxylation practice.

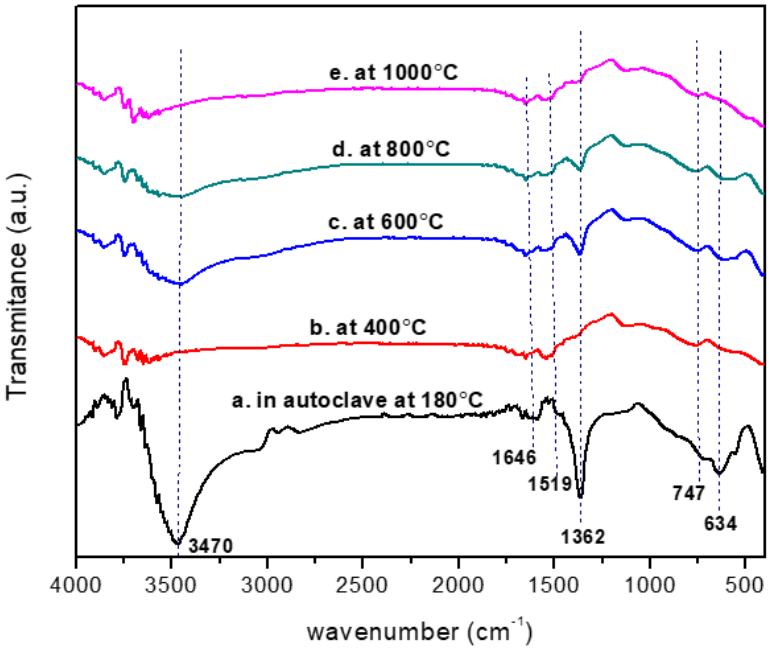

Figure 10. FTIR spectra of LDHs: **a)** autoclaved at 180ºC for 24 h; **(b), (c),** (**d**) and (**e**) calcined at 400, 600, 800, and 1000ºC, respectively.

The bands at 1519 and 1362 cm^{-1} are attributed to stretching vibrations of CO^{3-} ions [66-68]. The band intensity reduces with the rising temperature and converts into a small one at 1000 °C. This is owing to the elimination of intercalated CO^{3-} from the LDH structure [61].

The bands at 747-634 cm^{-1} seem to be allocated for Al–OH and Mg–OH translational modes [69]. Those bands are noticeably reduced and even disappear as the temperature increases to 1000 °C, signifying the collapse of Al–OH and Mg–OH translation modes after thermal treatment [70]. After increasing the temperature to more than 400°C, the decomposition of LDHs is started with the development of metal-oxides [61]. These results confirm the results achieved by XRD [63].

3.9. Particle shape and size of as-synthesized and calcined LDHs.

The particle shapes and sizes as well as their aggregation could be detected by SEM and TEM microscopy systems. Due to the specific structure of LDH, which contains inorganic anions in inter-layer structure with growing grains in a and b axes, this leads to the formation of hexagonal plate crystals [71].

Figs. 11 and 12 represent SEM images of LDHs as-synthesized using NaOH after autoclaving at 180ºC for 24h and that thermally-treated at 1000°C, respectively. The as-prepared LDH at 180°C (Figure 11) displays gel-like morphology with nanoparticles connected together, creating agglomerate. For the sample thermally treated at 1000 °C (Figure 12), grain growth occurred with the development of well-defined plate-like grains of 160 nm. The particles incline to form aggregates owing to their inherent properties [72- 75].

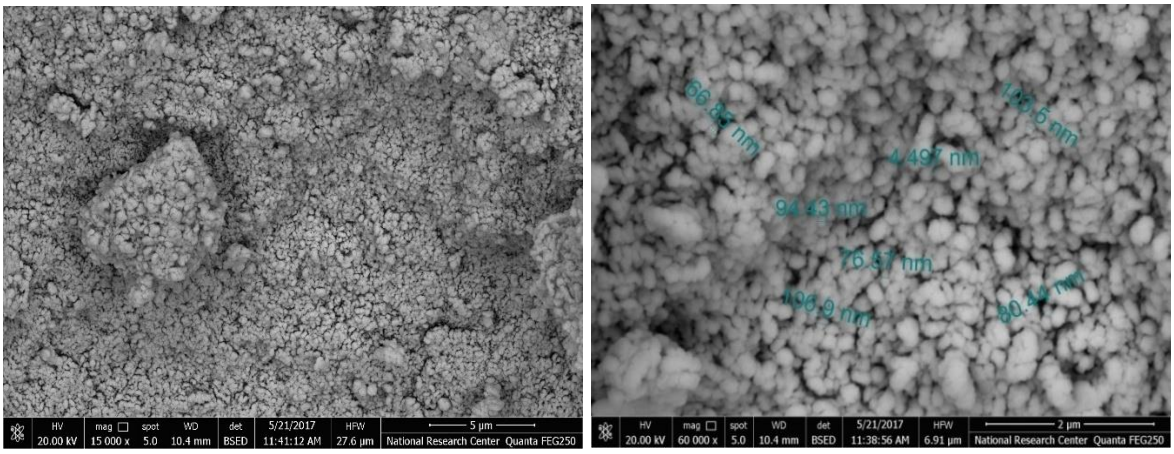

Figure 11. SEM images of as-synthesized LDH after autoclaving at 180ºC for 24 h (The inserted numbers indicate the diameters of small grains).

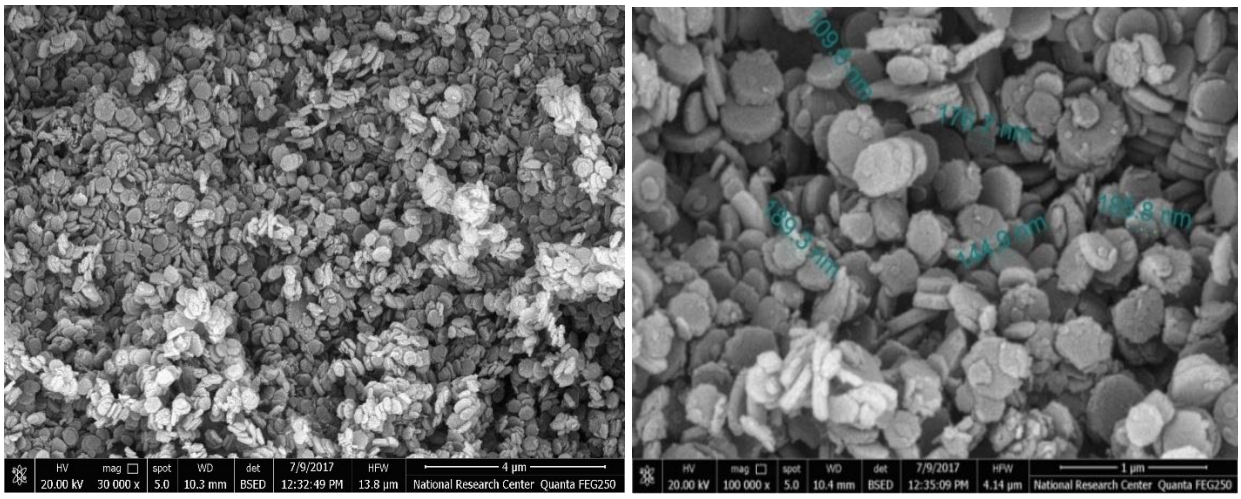

Figure 12. SEM images of LDH calcined at 1000ºC. (The inserted numbers indicate the diameters of small grains).

Figure 13 shows TEM images of as-synthesized LDH prepared using NaOH or NH4OH co-precipitated at 75°C (without hydrothermal treatment). It appears in Figure 13a that hexagonal-plate crystallites are noticed in the micrograph, which has a size of around 12.93 nm length and 1.12 nm diameter. The crystals have a remarkable tendency for particle-particle interaction, so the crystals appear from their edges [74,75]. The crystals seem to be relatively weekly formed due to the rapid reach of pH, and the reaction did not take enough time. On the other hand, TEM images of LDH prepared using NH4OH (Figure 13b) exhibit the formation of crystalline gibbsite with other intermediate phases.

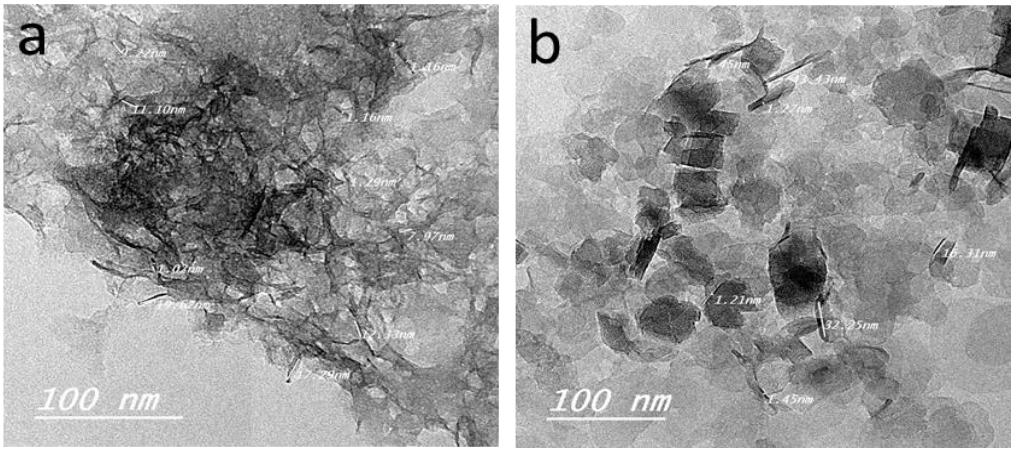

Figure 13. TEM images of as-synthesized LDHs (**a**) using NaOH and (**b**) using NH_4OH) co-precipitated at 75°C (without hydrothermal treatment).

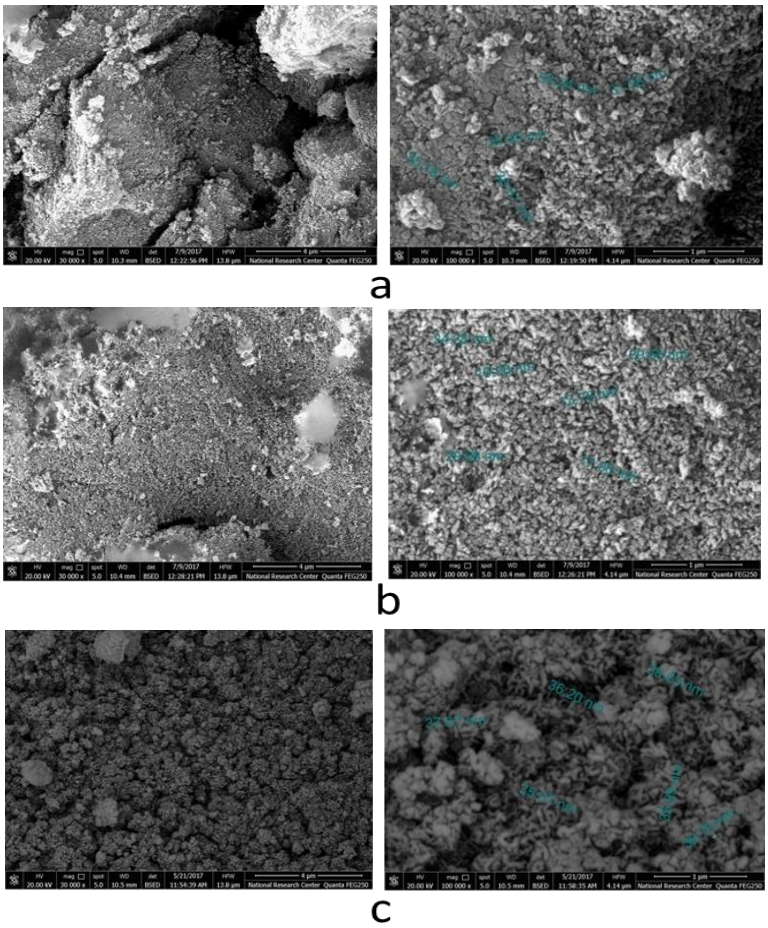

Figure 14. SEM images of as-synthesized LDHs doped with (**a)** 10, (**b)** 20, and (**c)** 30% Ni^{2+} after autoclaving at 180°C for 24 h (The inserted numbers indicate the diameters of small grains).

Figures 14 and 15 show SEM images of as-synthesized LDHs doped with 10%, 20%, and 30% Ni^{2+} or Co^{2+} after autoclaving at 180°C for 24 h, respectively. In these cases, a similar feature (morphology) to pure LDH is obtained, but particle sizes are different. They exhibit gel-like morphology with nanoparticles connected, creating agglomerates. The agglomeration in the case of LDH doped with Co^{2+} is much more condensed than that formed when LDH doped with Ni^{2+}. The average sizes of agglomerated grains are indicated in the Table. 4. Generally, adding Ni^{2+} or Co^{2+} causes a reduction in grain sizes. This indicates that these environments for synthesis lead to the formation of nanocrystalline materials due to their inherent properties [72-75]. This result confirms the result obtained by XRD.

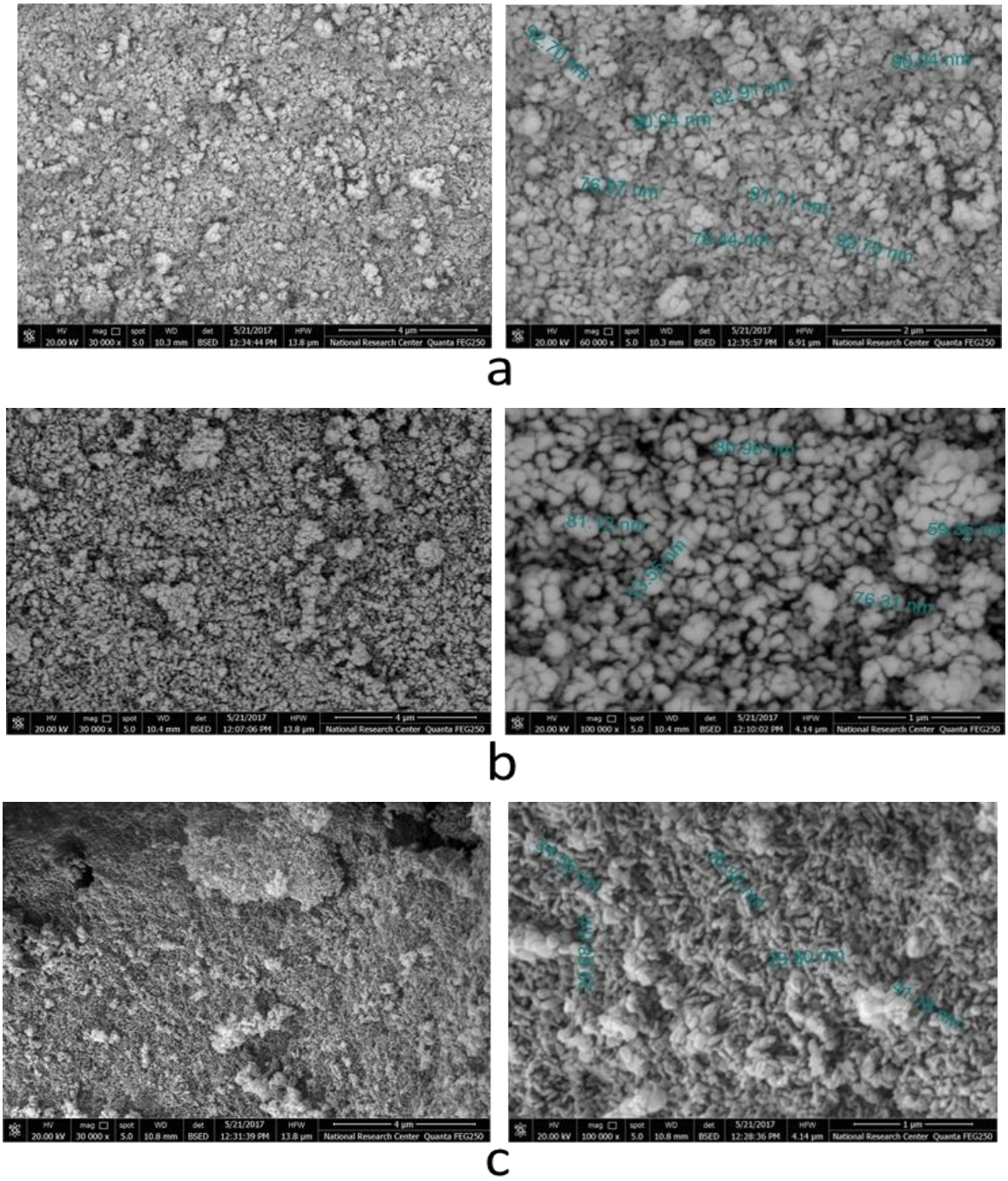

Figure 15. SEM images of as-synthesized LDHs doped with (**a)**10, (**b)**20, and (**c)** 30% Co^{2+} after autoclaving at 180°C for 24h.

Table 4. Average grain size of LDH agglomerated particles as calculated from SEM images.

No.	Sample identification	Sample formula	Average size, nm
1	as-synthesized LDH prepared using NaOH	$[Mg_{0.667}Al_{0.333}(OH)_{16}](CO_3)_{0.167}\cdot 4H_2O_{0.5}$	88.12
2	LDH calcined at 1000 °C	$MgAl_2O_4$	161.26
3	LDH doped with 10% Ni^{2+}	$[Mg_{0.567}Ni_{0.1}Al_{0.333}(OH)_{16}](CO_3)_{0.167}\cdot 4H_2O_{0.5}$	39.55
4	LDH doped with 20% Ni^{2+}	$[Mg_{0.467}Ni_{0.2}Al_{0.333}(OH)_{16}](CO_3)_{0.167}\cdot 4H_2O_{0.5}$	22.26
5	LDH doped with 30% Ni^{2+}	$[Mg_{0.367}Ni_{0.3}Al_{0.333}(OH)_{16}](CO_3)_{0.167}\cdot 4H_2O_{0.5}$	36.74
6	LDH doped with 10% Co^{2+}	$[Mg_{0.567}Co_{0.1}Al_{0.333}(OH)_{16}](CO_3)_{0.167}\cdot 4H_2O_{0.5}$	86.69
7	LDH doped with 20% Co^{2+}	$[Mg_{0.467}Co_{0.2}Al_{0.333}(OH)_{16}](CO_3)_{0.167}\cdot 4H_2O_{0.5}$	80.11
8	LDH doped with 30% Co^{2+}	$[Mg_{0.367}Co_{0.3}Al_{0.333}(OH)_{16}](CO_3)_{0.167}\cdot 4H_2O_{0.5}$	34.30

Figures 16 and 17 exhibit TEM images LDHs doped with 30% Ni^{2+} or Co^{2+} without hydrothermal treatment, respectively. It appears that homogenous grain morphology and sizes are detected in both LDHs. The grain size of LDH doped with Ni is smaller than that doped with Co. The grain size of LHD doped with Ni is about 10-25 nm, while that for LDH doped with Co is about 20-35nm.

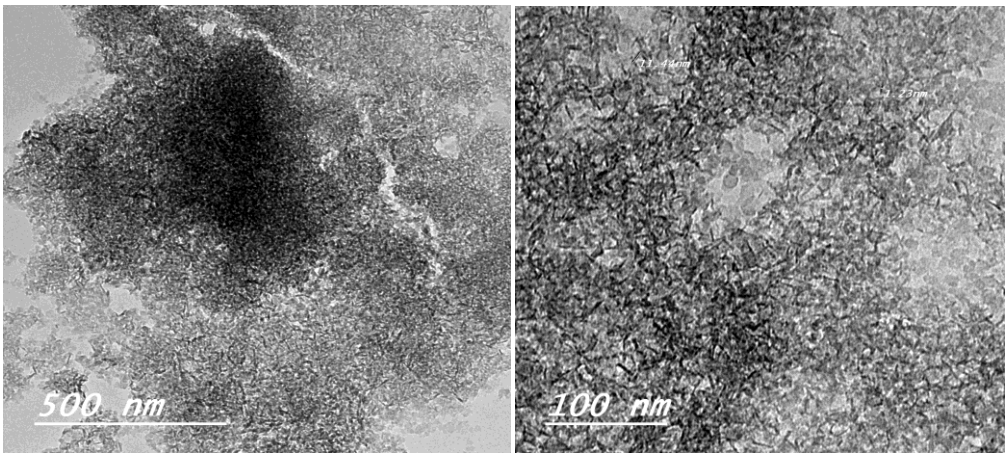

Figure 16. TEM images of LDH doped with 30% Ni^{2+} without hydrothermal treatment.

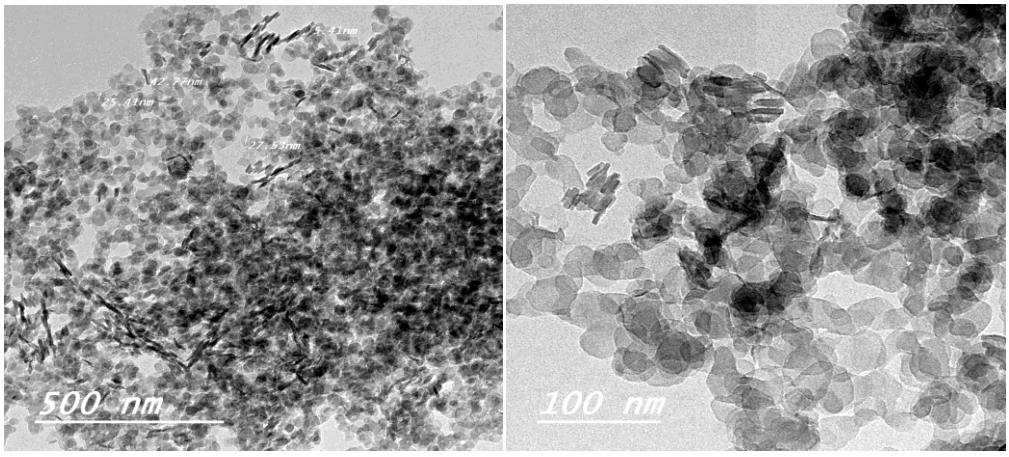

Figure 17. TEM images of LDH doped with 30% Co^{2+} without hydrothermal treatment.

3.11. Characteristics of sintered spinel prepared from LDHs.

LDHs have many attractive applications, especially in the ceramic area. Their applications in ceramics yield interesting class-named spinels such as $MgAl_2O_4$-$NiAl_2O_4$ and $MgAl_2O_4$-$CoAl_2O_4$ solid solutions with essential characteristics and applications like engineering materials, refractories, electronics, fusion-reactors, optical-devises and biomedical [24,25,33,76].

Generally, sintered Mg-A1 spinel is often prepared by solid-state reaction sintering between high-purity calcined MgO and calcined $A1_2O_3$ [77]. The sintering process usually needs a high temperature of more than 1600ºC, even if the starting materials are in submicron sizes [78]. The production of spinel from nanopowders reduces the sintering temperature and improves the properties of the products. The production of spinel powder through synthesized LDHs proceeds via several steps as follows:

Up to 250ºC, physically adsorbed water and interlayer water has been removed.

(2) In the range 250–600ºC, the layer structure collapses, and the LDH changes into mixed oxides-like phases due to de-hydroxylation to brucite-like (MgO) layers; and

(3) In the range 600-1000ºC, the mixed oxide decomposes to MgO and $MgAl_2O_4$ spinel due to the de-carbonation of interlayers and de-hydroxylation of the LDH.

The temperature of de-hydroxylation and de-carbonation, as well as the rate of thermal decomposition, depend on the mole fraction of M^{2+} [9,79]. In the present work, the decomposition of LDH during the calcination process leads to the formation of metal oxides M(II)O and spinel phases when the temperature is further increased to 1000 ºC. This calcination process increases the reactivity of powder and facilitates the formation of well-sintered spinel during the sintering at high temperatures. In the presented work, sintering of LDHs (doped and none doped with Co or Ni) synthesized from pure chemicals was conducted and investigated. Figure 18 shows images of sintered spinels prepared from synthesized LDHs.

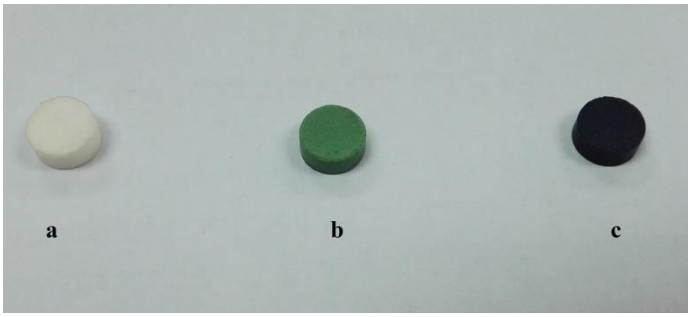

Figure 18. Images of spinels sintered at 1500ºC prepared using LDHs (a) pure spinel, (b) doped with 30% Ni and (c) doped with 30% Co.

3.11.1. Phase composition of spinel sintered at 1500ºC.

Figure 19 shows XRD patterns of pure spinel doped with 30% Co or 30% Ni sintered at 1500oC. From this figure, it appears that the general feature of the patterns indicating the presence of different forms of $MgAlO_4$, $MgNiAlO_4$, or $MgCoAlO_4$ spinels with some amounts of metal oxides, e.g., MgO, NiO, or CoO. Also, a little shift toward lower 2θ after the addition of transition metal is due to the differences in atomic radii between Mg^{2+}, Ni^{2+}, Co^{2+} ions. The spinels' characteristic peaks appeared at approximately 2θ equal 18.992, 31.298, 36.9, 44.859, 55.757, 59.458, and 65.314º (JCPDS file No. 96-900-3481), while the characteristic peaks of metal oxides appear at 2θ approximately equal 36.9, 43.087 and 62.589º. The spinel doped with

Co^{2+} prepared from pure chemicals exhibits the lowest crystallinity as indicated by their lower peak intensity (Figure 19c). This means the incomplete formation of spinel structure is detected, even after firing at 1500°C, which might reflect on the other properties as discussed later on. On the other side, pure spinels and others doped with Ni^{2+} exhibit well-crystalline materials after sintering at 1500°C. The crystallinity of spinel doped with 30% Ni^{2+} is the highest among other none doped or Co-doped spinels. Different parameters can affect the crystallinity of sintered materials, such as sintering temperature, purity of materials, crystal size, and crystallinity of starting materials.

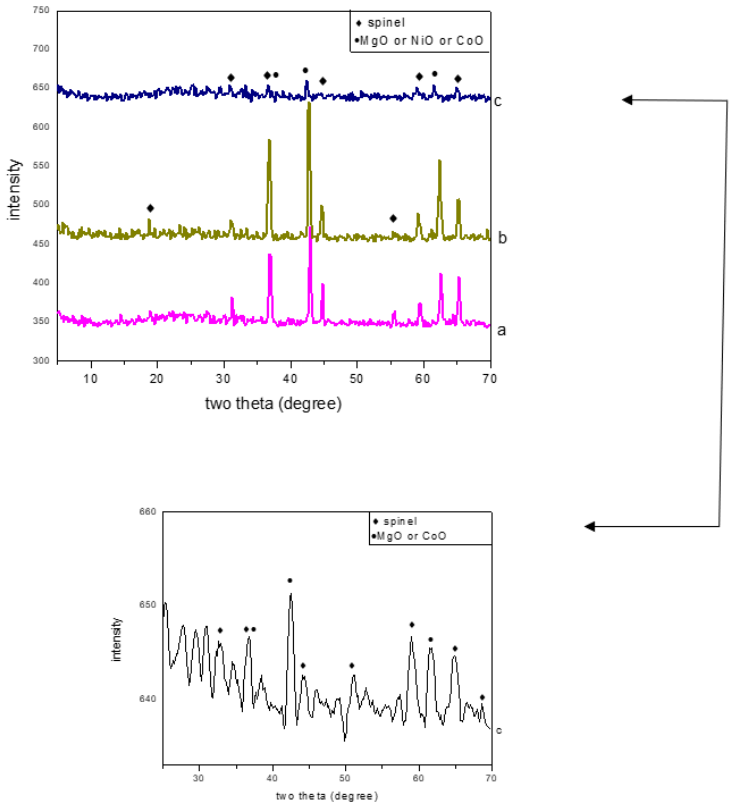

Figure 19. XRD patterns of spinel sintered at 1500°C; (**a)** pure spinel, (**b)** doped with 30% $Ni^{2+}$and (**c)** doped with 30% Co^{2+}.

In the present work, some of the aforementioned factors can affect the crystallinity and spinel formation in the cobalt sample. It needs a higher sintering temperature to complete spinel formation and increase the crystallinity. The probability of forming different oxidation states of cobalt might also have an additional effect on delaying the formation of crystalline spinel. The excess metal oxides indicated in XRD patterns are probably due to the changes in the stoichiometry of reactants (LDH) and products (spinels), or extra sintering temperature is needed to allow whole Mg^{2+}, Ni^{2+}, or Co^{2+} to enter the reaction completely. According to the general molecular structure of the LDH [(Mg or Co or Ni)$_6$Al$_2$(OH)$_{16}$CO$_3$·4H$_2$O] and spinels ($MgAl_2O_4$, $CoAl_2O_4$, and $NiAl_2O_4$), LDH has 6 divalent ions and 2 trivalent ions. In comparison, spinel has one divalent ion and 2 trivalent ions [25,36]. This means the sintering of LDH should give spinel with excess metal oxides (MgO, NiO, or CoO) after removing the hydroxides and carbonates in LDHs.

3.11.2. Bulk density and apparent porosity of sintered spinels.

It is worth mentioning that, during the preparation of sintered spinel using micro-sized starting materials, it is not easy to produce sintered spinel without pores when prepared by the

traditional sintering technique or without adding sintering aids. Thus, the production of spinel from nano-sized precursors could simplify the sintering with little amounts of pores formation. Furthermore, in the Mg-Al spinel system, the grain boundary mobility of the divalent metal rich-zone (e.g., Mg-rich zone) is higher than that of the Al-rich zone by about 100−300 times. Thus, spinel doped with transition metals, e.g., Ni or Co, might enable the grain-boundary mobility and sintering process by forming a solid spinel solution [25]. Table 5 illustrates the values of bulk density and apparent porosity of pure and doped spinels sintered at 1500°C. LDH gives sintered spinels at low temperatures better than when precursors are hydroxides/oxides of aluminum and magnesium. This is considered an interesting finding in the present work. Also, the sinterability is improved after the addition of Co^{2+} or Ni^{2+} as compared with pure spinels. As indicated from XRD results, the sintered materials compose of spinel plus relevant metal oxide as a result of the decomposition of LDH, which contains excess metal oxides than the stoichiometry of spinel. Thus, two factors can affect the sintering process. The first one is the density of both formed spinel and relevant metal oxide, while the second one is the densification process itself due to grain-grain interaction and diffusion after subjecting the material to heating at a suitable temperature and formation of spinel solid solution (spinel doped with Ni or Co). Considering the theoretical density of magnesium aluminate 3.65 g/cm^3, cobalt aluminate 4.26g/cm^3, nickel aluminate 3.44 g/cm^3, NiO 6.6 g/cm^3, CoO 6.11 g/cm3, MgO 3.58 g/cm^3, 30 % Co-containing magnesium aluminate (MgCoAl-spinel) 3.833 g/cm^3 and 30 % Ni-containing magnesium aluminate (MgNiAl-spinel) 3.587 g/cm^3, so, the obtained bulk density values of sintered materials are incomparable, and the densification of sintered materials can be followed up by the obtained apparent porosity or calculated relative density since it is difficult to calculate the exact relative density of sintered materials because the exact amount of each phase is not known. However, the relative density was calculated roughly according to the amount of phases obtained from the XRD semi-quantitative analysis (Table 6). The results of relative density are comparable with the values of measured apparent porosity. The apparent porosity decreases after the addition of cobalt and/or nickel. For the sintered materials, the obtained apparent porosity range is 4.4-3.1%. According to the apparent porosity results (Table 5), the best-densified bodies are the materials that contain nickel. These materials exhibit lower porosity and the best grain-grain interaction at 1500°C. In all cases, due to the formation of nanograins obtained after the decomposition of LDHs and the formation of sintered spinel ceramic, most of the formed pores are on the nanoscale. Satapathy [25,80] reported that the reduction of apparent porosity after adding few quantities of transition metals could be explained by the fact that this amount lies within the solubility limit of that material which improves the densification. For the double stages of the sintering process of spinel ceramics, the calcination of starting materials is also considered an important factor affecting the sintering process, where the conversion of the higher percentage of LDH into spinel and metal oxide might facilitate their sintering. Also, calcination can activate the materials and make them ready for sintering, but it might accelerate grain growth. This means that the developed spinel and metal oxides during calcination help to get better densification owing to the expansion of spinel unit-cell with the development of oxygen vacant-sites, i.e., spinel-structure develops anion deficient owing to the extra divalent cations as MgO or CoO or NiO [81-83].

Table 5. Bulk density and apparent porosity of spinels sintered at 1500°C.

No.	Material type	Apparent porosity, %	Bulk density, g/cm^3	Relative density, %
A	Spinel prepared from pure chemicals	4.415	3.45	94.52
B	Spinel doped with Co^{2+}, from pure chemicals	3.358	4.077	96.00
C	Spinel doped with Ni^{2+}, from pure chemicals	3.12	3.86	96.46

Table 6. Semi-quantitative analysis of sintered spinels as indicated from XRD results.

No.	Material type	Phase percentage, %	
A	Spinel prepared from pure chemicals	$MgAl_2O_4$ 46.4	MgO 53.6
B	Spinel doped with Co^{2+}, from pure chemicals	$MgAl_2O_4$-$CoAl_2O_4$ 65.3	MgO-CoO 34.7
C	Spinel doped with Ni^{2+}, from pure chemicals	$MgAl_2O_4$- $NiAl_2O_4$ (28.9+19.3=48.2)	MgO-NiO 51.8

3.11.3. Microstructure of sintered spinel.

SEM images of pure and doped spinels sintered at 1500°C are shown in Figure 20. Generally, the sintering of nanomaterials at high temperatures causes grain growth, but in the present work, sintered spinels with in situ formed nano-sized crystals agglomerated together are obtained as indicated in all SEM images. This might be due to the conversion of LDHs into spinel. This is considered an interesting finding in the present work. Also, free divalent ions hinder grain growth and control grain boundary migration [84]. Extra research studies are requested to understand the mechanism of this solid reaction and this interesting phenomenon for the conversion of LDH into spinels. For pure spinel (Figure 20), well-compact and dense microstructure with homogenous shape and size are obtained after sintering at 1500°C. Nano-sized grains are agglomerated together, forming micro-sized octahedron agglomerates. The size of nanograins is ranged between 50-100nm, while the size of agglomerates is ranged between 500-1200nm. The percentage of pores is decreased while the degree of compactness is increased after adding Co^{2+} or Ni^{2+}, with a slight change in the case of Ni^{2+}-containing spinel. The excess divalent metal oxides (Mg, Co, Ni) have appeared as bright grains that hinder grain growth.

4. Conclusions

The following remarks were concluded. The co-precipitation coupled with the hydrothermal method successfully prepared nano LDH powder up to 180oC. NaOH was more effective than NH4OH in the co-precipitation method. LDHs is considered an interesting precursor for production of sintered spinel with improved sinterability at lower temperature as compared with those prepared from micro-sized precursors as published in the literature. As previously mentioned, sintered bulk spinel fabrication through the conventional solid state method needs a higher temperature than the current studied method. As a new finding, the microstructure of sintered spinel was composed of nanograins agglomerated together, forming coarse grains. This can affect its mechanical properties when applied as a structural material. Doping of pure spinel Ni^{2+} and Co^{2+} led to improving the sinterability as compared with pure spinel.

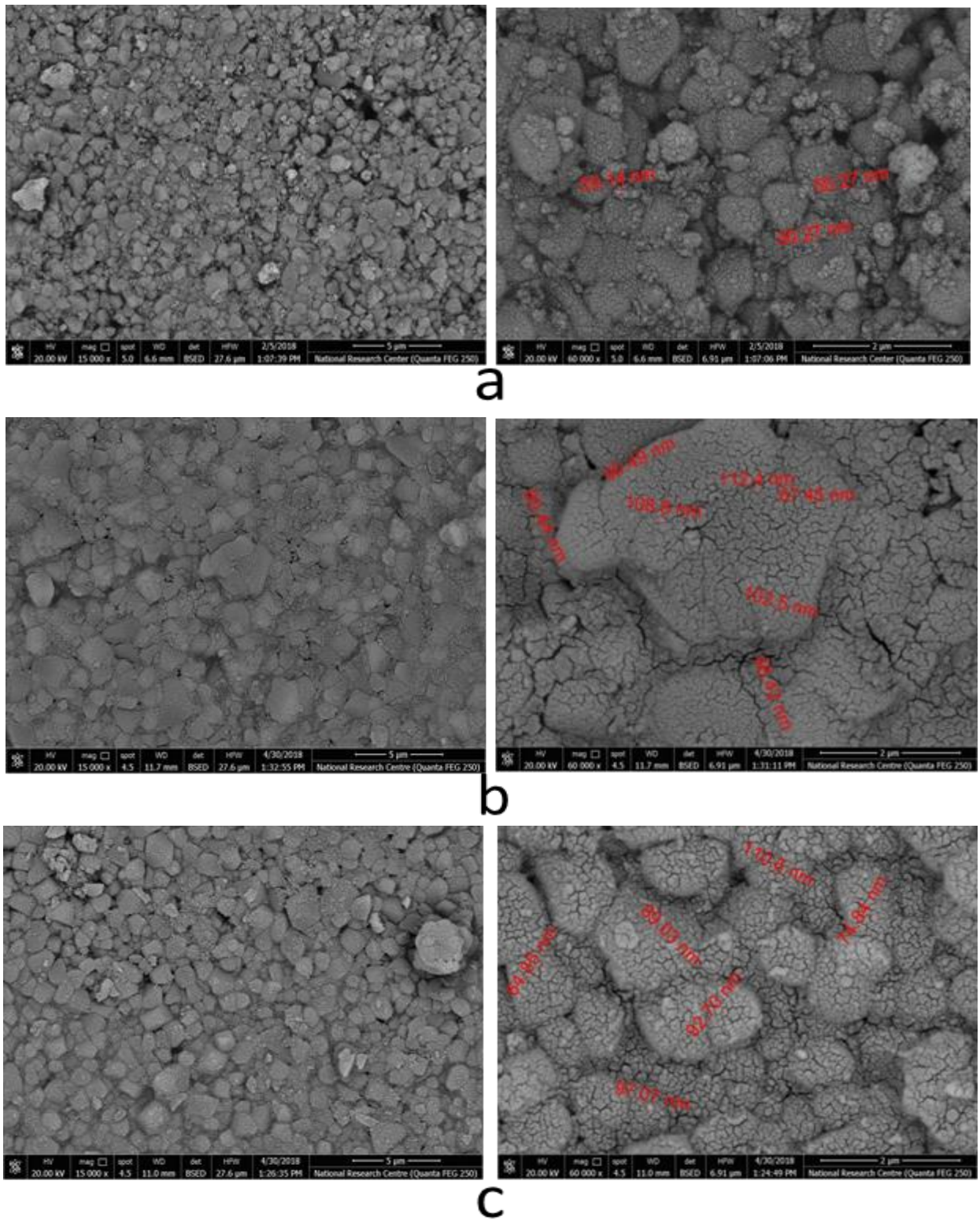

Figure 20. SEM images of spinel sintered at 1500ºC; **a)** pure spinel, **b)** doped with 30% Co^{2+}, and **c)** doped with 30% Ni^{2+} (The inserted numbers indicate the diameters of small grains)

Funding

This work has been funded by National Research Center, Egypt (MSc student grant).

Acknowledgments

This work has been supported by National Research Center, Egypt (MSc student grant).

Conflicts of Interest

The authors declare that they have no known competing financial interests or personal relationships that could have appeared to influence the work reported in this paper.

References

1. Bellotto, M.; Rebours, B.; Clause O.; Lynch, J.; Bazin, D.; Elkaim, E. Hydrotalcite Decomposition Mechanism: A Clue to the Structure and Reactivity of Spinel-like Mixed Oxides. *Physical Chemistry* **1996**, *100*, 8535-8542, https://doi.org/10.1021/jp960040i.
2. Richardson, M. C. Layered Double Hydroxides as Anion- and Cation-Exchanging Materials. Doctor of Philosophy (Inorganic Chemistry). *University of North Texas* **2007**, https://www.proquest.com/docview/304814805.
3. De Roy, A.; Forano, C.; El Malki, K.; Besse, J. P. Anionic clays: trends in pillaring chemistry. *In Expanded Clays and other microporous solids*, **1992**, 108-169, https://doi.org/10.1007/978-1-4684-8866-1_7.
4. Elaheh, Abdollahi; Azarakhsh, Heidari; Toraj Mohammadi; Amir AtabakAsadi; Maryam Ahmadzadeh Tofighy. Application of Mg-Al LDH nanoparticles to enhance flux, hydrophilicity and antifouling properties of PVDF ultrafiltration membrane: Experimental and modeling studies, *Separation and Purification Technology* **2021**, *257*, 117931, https://doi.org/10.1016/j.seppur.2020.117931.
5. Zubair, M.; Ihsanullah, I.; Hamidi, A.; Mohd, Azmier A.; Mamdouh, A. A. Sustainable wastewater treatment by biochar/layered double hydroxide composites: Progress, challenges, and outlook. *Bioresource technology* **2021**, *319*, 124128, https://doi.org/10.1016/j.biortech.2020.124128.
6. Manohara, G. V.; David Norris, M; Mercedes Maroto-Valer; Susana Garcia. Acetate intercalated Mg–Al layered double hydroxides (LDHs) through modified amide hydrolysis: a new route to synthesize novel mixed metal oxides (MMOs) for CO_2 capture. *Dalton Trans* **2021**, *50*. 7474, https://doi.org/10.1039/d1dt00602a.
7. Taylor, H. F. W. Crystal structures of some double hydroxide minerals. *Mineralogical Magazine* **1973**, *39*, 377-389, https://doi.org/10.1180/minmag.1973.039.304.01.
8. Allmann, R. The crystal structure of pyroaurite. *Acta Crystallographica* **1968**, *B24*, 972-977, https://doi.org/10.1107/S0567740868003511.
9. Bergaya, F.; Theng, B.K.G.; Lagaly G. Handbook of Clay Science, Chapter 13.1: Layered Double Hydroxides. *Developments in Clay Science* **2006**, *1*, 1021-1095, https://doi.org/10.1016/S1572-4352(05)01025-1.
10. Khattab, R.M.; Sadek, H.E.H.; Gaber, A.A.; Zawrah, M. F. Sinterability, physico-mechanical, electrical and magnetic properties of nano $Co_xMg_{1-x}Al_2O_4$ synthesized by microwave combustion method. *Ceramics International*, **2018**, *44*, 21525-21529, https://doi.org/10.1016/j.ceramint.2018.08.214.
11. Crepaldi, E.L.; Pavan, P.C.; Valim, J.B. Comparative Study of the Co-precipitation Methods for the Preparation of Layered Double Hydroxides. *J. Brazilian Chemistry Society* **2000**, *11*, 64-70, https://doi.org/10.1590/S0103-50532000000100012.
12. Marchi, A.J.; Apesteguía, C.R. Impregnation-induced memory effect of thermally activated layered double hydroxides. *Applied Clay Science* **1998**, *13*, 35-48, https://doi.org/10.1016/S0169-1317(98)00011-8
13. Rives, V. Characterization of layered double hydroxides and their decomposition products. *Materials Chemistry and Physics* **2002**, *75*, 19-25, https://doi.org/10.1016/S0254-0584(02)00024-X
14. Del, H C., Layered double hydroxides and human health: An overview. *Applied Clay Science* **2007**, *36*, 103-121, https://doi.org/10.1016/j.clay.2006.06.010.
15. Kaitao, L. I.; Guirong, W. A. N. G.; Dianqing, L. I.; Yanjun, L. I. N.; Xue, D. U. A. N. Intercalation assembly method and intercalation process control of layered intercalated functional materials. *Chinese Journal of Chemical Engineering* **2013**, *21*, 453-462, https://doi.org/10.1002/chin.201407243.
16. Zhao, Y., Li F.; Zhang, R.; Evans, D. G.; Duan, X. Preparation of layered double-hydroxide nanomaterials with a uniform crystallite size using a new method involving separate nucleation and aging steps. *Chemistry of Materials* **2002**, *14*, 4286-4291, https://doi.org/10.1021/cm020370h.
17. Kyung-Won Jung; Seon Yong Lee; Jae-Woo Choi; Min-Jin Hwang; Wang Geun Shim. Synthesis of Mg–Al layered double hydroxides-functionalized hydrochar composite via an in situ one-pot hydrothermal method for arsenate and phosphate removal: Structural characterization and adsorption performance. *Chemical Engineering Journal* **2021**, *420*, 129775, https://doi.org/10.1016/j.cej.2021.129775

18. Jaehyuk, K.; Tatiana, G. L; Sangsu P.; Jueun K.; Tamas V.; Wooyong U. Nanostructured MgFe and CoCr Layered Double Hydroxides for Removal and Sequestration of Iodine Anions. *Chemical Engineering Journal* **2020**, *380*, 122408, https://doi.org/10.1016/j.cej.2019.122408.
19. Almanassra, I. W.; Gordon M; Viktor K.; Muataz A. A.; Tareq A. A state of the art review on phosphate removal from water by biochars. *Chemical Engineering Journal* **2021**, *409*, 128211, https://doi.org/10.1016/j.cej.2020.128211
20. Weerasundara, L.; Yong-Sik O.; Jochen B. Selective removal of arsenic in water: A critical review. *Environmental Pollution* **2021**, *268*, 115668, https://doi.org/10.1016/j.envpol.2020.115668
21. Tichit, D.; Ribet, S.; Coq, B. Characterization of calcined and reduced multicomponent Co-Ni-Mg-Al-layered double hydroxides. *European Journal of Inorganic Chemistry* **2001**, *2*, 539–546, https://doi.org/10.1002/1099-0682(200102)2001:2%3C539::AID-EJIC539%3E3.0.CO;2-R
22. Lee, S. Y.; Kyung-Won, J; Jae-Woo, C; Young Jae L. In situ synthesis of hierarchical cobalt-aluminum layered double hydroxide on boehmite surface for efficient removal of arsenate from aqueous solutions: effects of solution chemistry factors and sorption mechanism. *Chemical Engineering Journal* **2019**, *368*, 914-923, https://doi.org/10.1016/j.cej.2019.03.043
23. Sadek, H.E.H.; Khattab, R. M.; Gaber, A. A.; Zawrah, M.F. Nano $Mg_{1-x}Ni_xAl_2O_4$ spinel pigments for advanced applications, *Spectrochimica, Acta Part A: Molecular and Biomolecular Spectroscopy* **2014**, *125*, 353–358, https://doi.org/10.1016/j.saa.2014.01.115.
24. Zawrah, M F; Serry, M. A.; Schneider, J; Zum Gahr, K-H. Microstructure and Mechanical Properties of Non-Stoichiometric $MgAl_2O_4$-Spinel Bodies. *Cfi/Ber. DKG* **2000**, *77*, https://www.researchgate.net/publication/286837378_As_Microstructure_and_mechanical_properties_of_non-stoichiometric_MgAl2O4_spinel_bodies.
25. Serry, M. A.; Hammad, S. A.; Zawrah, M F. Phase Composition and Microstructure of Refractory $MgAl_2O_4$ Spinel Grains. *Brit. Ceramic Trans* **1998**, *97*, 275-282,
26. Nuernberg, G. D.; Foletto, E. L.; Probst, L. F.; Campos, C. E.; Carreño, N. L.; Moreira, M. A. A novel synthetic route for magnesium aluminate ($MgAl_2O_4$) particles using metal-chitosan complexation method. *Chemical engineering journal* **2012**, *193*, 211-214, https://doi.org/10.1016/j.cej.2012.04.054.
27. Canova, F. F.; Foster, A. S., Rasmussen M. K., Meinander K., Besenbacher F., Lauritsen J.V. Non-contact atomic for cemicroscopy study of hydroxyl groups on the spinel $MgAl_2O_4$ (100) surface. *Nanotechnology* **2012**, *23*,1-13, https://doi.org/10.1088/0957-4484/23/32/325703.
28. Mosayebi, Z.; Rezaei, M.; Hadian, N.; Kordshuli, F.Z.; Meshkani F. Low temperature synthesis of nanocrystalline magnesium aluminate with high surface area by surfactant assisted precipitation method: effect of preparation conditions. *Materials Research Bulletin* **2012**, *47*, 2154–60, https://doi.org/10.1016/j.materresbull.2012.06.010.
29. Ganesh, I. A review on magnesium aluminate ($MgAl_2O_4$) spinel: synthesis, processing and applications. *International Materials Reviews* **2013**, *58*, 63–112, https://doi.org/10.1179/1743280412Y.0000000001
30. Ismail, B.; Hussain, S.T.; Akram, S. Adsorption of methylene blue onto spinel magnesium aluminate nanoparticles: adsorption isotherms, kinetic and thermodynamic studies. *Chemical Engineering* **2013**, *219*, 395–402, https://doi.org/10.1016/j.cej.2013.01.034
31. Klym, H.; Ingram, A.; Hadzaman, I.; Shpotyukde, O. Evolution of porous structure and free volume entities in magnesium aluminate spinel ceramics. *Ceramics International* **2014**, *40*, 8561–8567, https://doi.org/10.1016/j.ceramint.2014.01.070.
32. Lallemant, L.; Petit, J.; Lalanne, S.; Landais, S.; Trombert, S.; Vernhet L. Modeling of the green body drying step to obtain large size transparent magnesium-aluminate spinel samples. *European Ceramic Society* **2014**, *34*, 791-9, https://doi.org/10.1016/j.jeurceramsoc.2013.10.003.
33. Orosco, P.; Barbosa, L.; Ruiz, M.D. Synthesis of magnesium aluminate spinel by periclase and alumina chlorination. *Materials Research Bulletin* **2014**, *59*, 337-340, https://doi.org/10.1016/j.materresbull.2014.07.026.
34. Al-Hazmi, F.S.; Mahmoud, W.E. Poly (N-isopropyl acrylamide) assisted microwave synthesis of magnesium aluminate spinel oxide for production of highly trans-parent films by hot compression. *European Ceramic Society* **2014**, *34*, 3047-50, https://doi.org/10.1016/j.materresbull.2014.07.026.
35. Nassar, M. Y.; Ahmed, I. S.; Samir, I. A novel synthetic route for magnesium aluminate ($MgAl_2O_4$) nanoparticles using sol–gel auto combustion method and their photocatalytic properties, *Spectrochimica Acta Part A: Molecular and Biomolecular Spectroscopy* **2014**, *131*, 329-334, https://doi.org/10.1016/j.saa.2014.04.040.

36. Tang, C.; Zhai, Z.; Li, X.; Sun, L.; Bai, W. Sustainable production of acetaldehyde from lactic acid over the magnesium aluminate spinel, *Journal of the Taiwan Institute of Chemical Engineers* **2016**, *58*, 97-106, https://doi.org/10.1016/j.jtice.2015.06.014.
37. Porta, P.; Stone, F. S.; Turner, R. G. The distribution of nickel ions among octahedral and tetrahedral sites in $NiAl_2O_4$-$MgAl_2O_4$ solid solutions. *Solid State Chemistry* **1974**, *11*, 135-147 ,https://doi.org/10.1016/0022-4596(74)90108-X.
38. Jacob, K.T.; Alcock, C.B. Activities and their relation to cation distribution in $NiAl_2O_4$-$MgAl_2O_4$ spinel solid solutions. *Solid State Chemistry* **1977**, *20*, 79-88. https://doi.org/10.1016/0022-4596(77)90053-6.
39. Po-Hsiang, C.; Zhaohui, L.; Wei-Teh J. Calcination of hydrotalcite to enhance the removal of perfluorooctane sulfonate from water. *Applied Clay Science* **2020**, *190*, 105563, https://doi.org/10.1016/j.clay.2020.105563.
40. Zawrah, M. F. Investigation of lattice constant, sintering and properties of nano Mg–Al spinels. *Materials Science and Engineering: A* **2004**, *382*, 362–370, https://doi.org/10.1016/j.msea.2004.05.074.
41. Rafael, S.; Mariana, O.C.; Villas B.; Victor, C. P. Porous alumina-spinel ceramics for high temperature applications. *Ceramics International* **2011**, *37*, 1393–1399, https://doi.org/10.1016/j.ceramint.2011.01.012.
42. Arruda, C.C.; Cardoso, P.H.L.; Dias, I.M.M.; Salomão, R. Hydrotalcite ($Mg_6Al_2(OH)_{16}(CO_3)\cdot 4H_2O$) A potentially useful raw material for refractories. *Interceram Refractories Manual* **2013**, *62*, 187-191.
43. Nacera, B.; Hafida M.,;Djamila B.; Mehdi A.; Abdelkader T., Agustin Fortuny, Hary Demey, Ana Maria Sastre. Removal of Zinc from Aqueous Solutions Using Lamellar Double Hydroxide Materials Impregnated with Cyanex 272: Characterization and Sorption Studies. *Molecules* **2020**, *25* , 1263, https://doi.org/10.3390/molecules25061263.
44. Schaper, H.; Berg-Slot, J.J.; Stork, W.H.J. Stabilized magnesia: a novel catalyst (support) material. *Applied Catalysis* **1989**, *54*, 79-90, https://doi.org/10.1016/S0166-9834(00)82356-8.
45. Vithanage, M.; Ahmed A.; Sammani R.; Amit B. Implications of layered double hydroxides assembled biochar composite in adsorptive removal of contaminants: Current status and future perspectives. *Science of The Total Environment* **2020**, *737*, 139718, https://doi.org/10.1016/j.scitotenv.2020.139718.
46. Yuecen D.; Xiangrui K.; Xingshen L.; Hongtao W. Adsorptive removal of heavy metal anions from water by layered double hydroxide: A review. *Chemosphere* **2022**, *303*,134685, https://doi.org/10.1016/j.chemosphere.2022.134685.
47. Hall, W.H. X-Ray line broadening in metals. *Proceedings of the Physical Society of London* **1949**, *62*, 741-743, https://iopscience.iop.org/article/10.1088/0370-1298/62/11/110.
48. Klung, H.P.; Alexander, L.E. X-ray Diffraction Procedures for Polycrystalline and Amorphous Materials, 2nd edition, John Wiley & Sons, New York **1974**, https://doi.org/10.1002/xrs.1300040415.
49. Khattab, R.M.; Sadek, H.E.H.; Gaber, A.A. Microwave Synthesis of $Co_xMg_{1-x}Al_2O_4$ Seed for Pigment Application. *Interceram-International Ceramic Review* **2016**, *65*, 106-110, https://doi.org/10.1007/BF03401160.
50. Wenxian G.; Xiaoming, W.; Mengqiang, Z.; Dong-Xing, G.; Xinxin M.; Hongtao, W.; Wei, L. Long-Range and Short-Range Structures of Multimetallic Layered Double Hydroxides. *The Journal of Physical Chemistry C* **2022**, *126*, 5311-5322, https://doi.org/10.1021/acs.jpcc.2c00121.
51. Liao, L.; Zhao, N.; Xia, Z. Hydrothermal synthesis of Mg–Al layered double hydroxides (LDHs) from natural brucite and $Al(OH)_3$. *Materials Research Bulletin* **2012**, *47*, 3897–3901, https://doi.org/10.1016/j.materresbull.2012.07.007.
52. Kovanda, F.; Koloušek, D.; Cílová, Z.; Hulínský, V. Crystallization of synthetic hydrotalcite under hydrothermal conditions. *Applied clay science* **2005**, *28*, 101-109, https://doi.org/10.1016/j.clay.2004.01.009.
53. Yuwen, L.; Fengyun, D.; Linsen, Z.; Kela X.; Chao L.; Peilong L.; Zexuan Z.; Cun H.; Yan S.; Jiangfeng, S.; Huaiqiang Z.; Xin Z. Methane decomposition to high-quality carbon nanotubes: well-distributed NiCo alloy catalysts derived from layered double hydroxide. *Journal of Materials Science* **2022**, *57*, 11783-11795, https://doi.org/10.1007/s10853-022-07339-w.
54. Hickey, L.; Kloprogge, J.T.; Frost, R.L. The effects of various hydrothermal treatments on magnesium-aluminum layered double hydroxides. *Material Science* **2000**, *35*, 4347-4355, https://doi.org/10.1023/A:1004800822319.
55. Zawrah, M. F. Characterization and Sinterability of Chemically Precipitated Phosphate-Bearing Magnesia Grains. *Ceramics International* **2001**, *27*, 523–529, https://doi.org/10.1016/S0272-8842(00)00111-5.
56. Natalia, N. L.; Svetlana V. C.; Liudmila, N.; Stepanova, V.; Drozdov A.; Aleksandr, V. L. Structural Aspects of "Memory Effect" for MgGa LDHs: New Data Obtained by Simulation of XRD Patterns for 1D Disordered Crystals. *Crystals* **2022**, *12*, 629, https://doi.org/10.3390/cryst12050629.

57. Zawrah, M. F.; El Kheshen, A. A. Synthesis and Characterization of Nanocrystallite $MgAl_2O_4$ Ceramics Powders by use of molten salts. *British ceramic transactions* **2002**, *101*, 71-74, https://doi.org/10.1179/096797801225000888.
58. Zawrah, M. F.; Meky, S. Synthesis and Characterization of Nano $MgAl_2O_4$ Spinel by Co-precipitated Method. *Ceramics International* **2007**, *33*, 969–978, https://doi.org/10.1016/j.ceramint.2006.02.015.
59. Miri, K.; Inseon O.; Hyunkyung C.; Wonsik, J.; Jaejung, S.; Chul, S. K.; Jung-Woo Y.; Seungho C. A solution-based route to compositionally complex metal oxide structures using high-entropy layered double hydroxides. *Cell Reports Physical Science* **2022**, *3*, 100702, https://doi.org/10.1016/j.xcrp.2021.100702.
60. Karina W.; Dominika, M. Synthesis and evaluation of Mg-Al hydrotalcite formation and 2002, its influence on the microstructural evolution of spinel-forming refractory castables under intermediate temperatures. *Journal of the European Ceramic Society* **2022**, *42*, 2545-2555, https://doi.org/10.1016/j.jeurceramsoc.2022.01.009.
61. Meriem, D.; Mostefa K.; Hakima, K.; Mohamed M. B.; Abdellah B. Synthesis of nickel-based layered double hydroxide (LDH) and their adsorption on carbon felt fibres: application as low cost cathode catalyst in microbial fuel cell (MFC). *Environmental Technology* **2021**, *42*, 492-504, https://doi.org/10.1080/09593330.2019.1635652.
62. Yufeng, C. H. E. N.; Yao, B. A. O.; Zhipeng, Y. U.; Guangchao, Y. A. N. G.; Xiaoqing, W. A. N. G. Photoluminescence of Tb-doped MgAl-LDHs depending on phase transition caused by annealing. *Rare Earths* **2016**, *34*, 36-44, https://doi.org/10.1016/S1002-0721(14)60575-5.
63. Kasprzyk-Hordern, B. Chemistry of alumina, reactions in aqueous solution and its application in water treatment *Advances in Colloid and Interface Science* **2004**, *110*, 19–48, https://doi.org/10.1016/j.cis.2004.02.002.
64. Wang, J.; Liu, Q.; Zhang, G.C.; Li, Z.S.; Yang, P.P.; Jing, X.Y.; Zhang, M.L.; Liu, T.F.; Jiang, Z. Synthesis, sustained release properties of magnetically functionalized organic– inorganic materials: amoxicillin anions intercalated magnetic layered double hydroxides via calcined precursor at room temperatures. *Solid State Sciences* **2009**, *11*, 1597-1601, https://doi.org/10.1016/j.solidstatesciences.2009.06.015.
65. Chen, Y.F; Zhou, S.H.; Li, F.; Wei, J.C.; Dai, Y.F.; Chen, Y.W. Fluorescence and phase transitions of Mg-Al-Eu ternary layered double hydroxides dependence on annealing *Clay Minerals* **2011**, *46*, 487-493, https://doi.org/10.1180/claymin.2011.046.3.487.
66. Yilin, Z.; Peng, Z.; Jing, X.; Yuechang, W.; Ning, J.; Yuanfeng, L.; Hongjie, C.; Zhen, Z.; Jian, L.; Jinqing J. Synergistic effect of binary Co and Ni cations in hydrotalcite-derived $Co_{2-x}Ni_xAlO$ catalysts for promoting soot combustion. *Fuel* **2022**, *320*, 123888, https://doi.org/10.1016/j.fuel.2022.123888.
67. Poudel, M. B.; Miyeon, S.; Han, J. K. "Interface engineering of MIL-88 derived MnFe-LDH and $MnFe_2O_3$ on three-dimensional carbon nanofibers for the efficient adsorption of Cr (VI), Pb (II), and As (III) ions. *Separation and Purification Technology* **2022**, *287*, 120463, https://doi.org/10.1016/j.seppur.2022.120463.
68. Wahsh, M. M. S.; Khattab, R. M.; Zawrah, M. F. Alumina/zirconia ceramic membranes fabricated by temperature induced forming technique, Ceramics International. *Ceramics International* **2022**, *48*, 26460–26465, https://doi.org/10.1016/j.ceramint.2022.05.340.
69. Delgado, R.R.; Pauli, C.P.D.; Carrasco, C.B.; Avena, M.J. Influence of MII/MIII ratio in surface-charging behavior of Zn-Al layered double hydroxides. *Applied Clay Science* **2008**, *40*, 27-37. https://doi.org/10.1016/j.clay.2007.06.010.
70. Zhou, J.; Zhaoyang, L.; Huaying, R.; Xidong, D.; Imran, S.; Yu H.; Xiangfeng, D. Layered intercalation materials. *Advanced Materials* **2021**, *33*, 2004557, https://doi.org/10.1002/adma.202004557.
71. Zawrah, M. F.; El Defrawy, S. A; Omyma, A. M. A.; Sadek, H. E. H.; Eman, E. G. Recycling of LCW produced form water plants for synthesizing of nano FeO(OH), $Al(OH)_3$, and layered double hydroxide: Effect of heat-treatment. *Ceramics International* **2018**, *44*, 9950-9957, https://doi.org/10.1016/j.ceramint.2018.03.025.
72. Zawrah, M. F. Synthesis and characterization of WC-Co nanocomposites by novel chemical method. *Ceramics International* **2007**, *33*, 155–161, https://doi.org/10.1016/j.ceramint.2005.09.010.
73. Zawrah, M. F.; Khalil, N. Synthesis and characterization of calcium aluminate nano ceramic powders for new applications. *Ceramics International* **2007**, *33*, 1419–1425, https://doi.org/10.1016/j.ceramint.2006.04.022.
74. Rabab, K. K.; Wahba, M. A; Badry, M. D.; Zawrah, M.F.; Heikal, E. Highly ordered pure and indium-incorporated MCM-41 mesoporous adsorbents: Synthesis, characterization and evaluation for dye-removal. *Journal of Materials Science* **2022**, *57*, 4504–4527, https://doi.org/10.1007/s10853-022-06877-7.

75. El Rafie, A.M.; Zawrah, M.F. Effect of Alkali Concentration and Reaction Time on the Morphology of ZnO Nano-Microparticles Prepared by Hydrothermal Method. *Ceramic Science and Technology* **2014**, *05*, 193–198, https://doi.org/10.4416/JCST2014-00002.
76. Zawrah, M. F.; Serry, M. A.; Gahr, K-Z. Mechanical properties of co-precipitated MgO-Al_2O_3 refractories as related to their phase composition and microstructure. *In CFI Ceramic forum international* **1999**, *76*, 36-39, https://pascal-francis.inist.fr/vibad/index.php?action=getRecordDetail&idt=1830985.
77. Tripathi, H.S.; Singla, S.; Ghosh, A. Synthesis and densification behaviour of magnesium aluminate spinel: Effect of Dy_2O_3. *Ceramics International* **2009**, *35*, 2541-2544, https://doi.org/10.1016/j.ceramint.2009.02.011.
78. Vineet, S.; Allan, S. Hydration and microstructural characteristics of MgO in the presence of metakaolin and silica fume. *Cement and Concrete Composites* **2021**, *121*, 104068. https://doi.org/10.1016/j.cemconcomp.2021.104068.
79. Cherepanova, S. V.; Leont'eva, N. N.; Arbuzov, A. B.; Drozdov, V. A.; Belskaya, O. B.; Antonicheva, N. V. Structure of oxides prepared by decomposition of layered double Mg–Al and Ni–Al hydroxides. *Solid State Chemistry* **2015**, *225*, 417-426, https://doi.org/10.1016/j.jssc.2015.01.022.
80. Zhang, Y.; Junkai, W.; Junfeng C.; Yawei, L.; Zhengliang X. Reconstruction and hydration of hydrotalcite response to thermal activation temperature: Enhancement of properties for magnesia castables. *Ceramics International* **2022**, *48*, 31245-31254, https://doi.org/10.1016/j.ceramint.2022.06.199.
81. Dominika, M.; Karina, T. In Situ Spinel Formation in a Smart Nano-Structured Matrix for No-Cement Refractory Castables. *Materials* **2020**, *13* , 1403, https://doi.org/10.3390/ma13061403.
82. Mohapatra, D.; Sarkar, D. Preparation of MgO–$MgAl_2O_4$ composite for refractory application. *Materials Processing Technology* **2007**, *189*, 279-283, https://doi.org/10.1016/j.jmatprotec.2007.01.037.
83. Khattab, R.M.; EL-Rafei, A.M.; Zawrah, M.F. In situ formation of sintered cordierite–mullite nano–micro composites by utilizing of waste silica fume. *Materials Research Bulletin* **2012**, *47*, 2662–2667, https://doi.org/10.1016/j.materresbull.2012.04.036.
84. Kenya, H.; Tadashi, O.; Zenbee, N. Effects of starting materials and calcining temperature on sintering of spinel ceramics. *Rep. Res. Lab. Eng. Mater. Tokyo Institute of Technology* **1977**, *2*, 85–94, https://doi.org/10.1007/s41779-017-0114-y.